HNF1A and A1CF coordinate a beta cell transcription-splicing axis that is in 2 diabetes

Bernardo, E.; Vas, M.G.; Balboa, D.; Cuenca-Ardura, M.; Bonàs-Guarch, S.; Planas-Fèlix, M.; ... ; Ferrer, J.

Cell Metabolism

Article

HNF1A and A1CF coordinate a beta cell transcription-splicing axis that is disrupted in type 2 diabetes

Graphical abstract

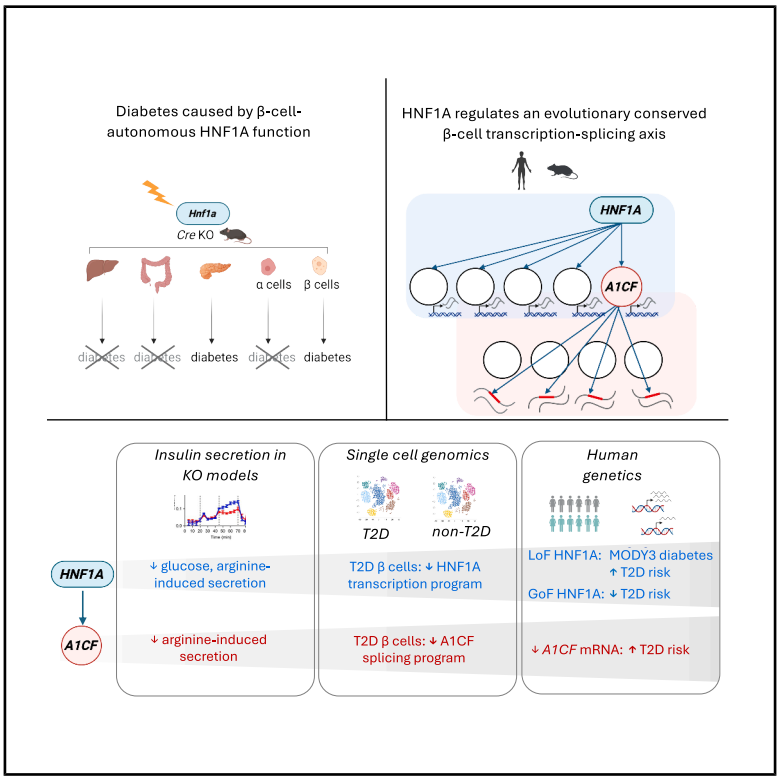

Highlights

- HNF1A-deficient diabetes arises from a β cell-autonomous defect
- HNF1A and A1CF coordinate a β cell transcription and splicing program
- Individuals with T2D exhibit increased β cells with suppressed *HNF1A-A1CF* axis
- Decreased islet *A1CF* expression is associated with increased glycemia and T2D risk

Authors

Edgar Bernardo, Matías Gonzalo De Vas, Diego Balboa, ..., Santiago Vernia, Patrik Rorsman, Jorge Ferrer

Correspondence

jorge.ferrer@crg.eu

In brief

Bernardo et al. uncover a transcription-splicing regulatory axis driven by HNF1A and A1CF in pancreatic β cells. Targeted perturbations, single-cell studies, and human genetic evidence demonstrate that failure of this network leads to defective β cell function and glucose homeostasis.

Bernardo et al., 2025, Cell Metabolism *37*, 1870–1889
September 2, 2025
https://doi.org/10.1016/j.cmet.2025.07.007

CellPress

CellPress
OPEN ACCESS

Cell Metabolism

Article

HNF1A and A1CF coordinate a beta cell transcription-splicing axis that is disrupted in type 2 diabetes

Edgar Bernardo,[1,2,18] Matías Gonzalo De Vas,[3,18] Diego Balboa,[1,2,17,19] Mirabai Cuenca-Ardura,[1,2,19] Sílvia Bonàs-Guarch,[1,2,3,19] Mercè Planas-Fèlix,[1,2,19] Fanny Mollandin,[1,2,19] Miquel Torrens-Dinarès,[1,2] Miguel Angel Maestro,[1,2] Javier García-Hurtado,[1,2] Sonia Moratinos,[1,2] Philippe Ravassard,[4] Haiqiang Dou,[5] Holger Heyn,[6] Alexander van Oudenaarden,[7,8,9] Nathalie Groen,[10,16] Eelco de Koning,[10,16] Christian Conrad,[11] Roland Eils,[11,12] Santiago Vernia,[13,14] Patrik Rorsman,[5,15] and Jorge Ferrer[1,2,3,20,*]

[1]Centre for Genomic Regulation, the Barcelona Institute of Science and Technology, Barcelona, Spain
[2]Centro de Investigación Biomédica en Red Diabetes y Enfermedades Metabólicas Asociadas (CIBERDEM), Barcelona, Spain
[3]Section of Genetics and Genomics, Department of Metabolism, Digestion and Reproduction, Imperial College London, London, UK
[4]Paris Brain Institute, Sorbonne Université, Inserm U1127, CNRS UMR 7225, Paris, France
[5]Department of Physiology, Sahlgrenska Academy, University of Gothenburg, Gothenburg, Sweden
[6]Centro Nacional de Análisis Genómico (CNAG), Barcelona, Spain
[7]Oncode Institute, Utrecht, the Netherlands
[8]Hubrecht Institute-KNAW, Utrecht, the Netherlands
[9]University Medical Center Utrecht, Utrecht, the Netherlands
[10]Hubrecht Institute, Royal Netherlands Academy of Arts and Sciences, and University Medical Center, Utrecht, the Netherlands
[11]Berlin Institute of Health at Charité – Universitätsmedizin Berlin, Center of Digital Health, Berlin, Germany
[12]Health Data Science Unit, Heidelberg University Hospital and BioQuant, Heidelberg, Germany
[13]MRC Laboratory of Medical Sciences (LMS), London, UK
[14]Institute of Clinical Sciences (ICS), Faculty of Medicine, Imperial College, London, UK
[15]Oxford Centre for Diabetes, Endocrinology and Metabolism, University of Oxford, Churchill Hospital, Oxford, UK
[16]Department of Medicine, Leiden University Medical Center, Leiden, the Netherlands
[17]Present address: Stem Cells and Metabolism Research Program, Faculty of Medicine, University of Helsinki, Helsinki, Finland
[18]These authors contributed equally
[19]These authors contributed equally
[20]Lead contact
*Correspondence: jorge.ferrer@crg.eu
https://doi.org/10.1016/j.cmet.2025.07.007

SUMMARY

Type 2 diabetes (T2D) is a devastating chronic disease marked by pancreatic β cell dysfunction and insulin resistance, whose pathophysiology remains poorly understood. *HNF1A*, which encodes transcription factor hepatocyte nuclear factor-1 alpha, is the most commonly mutated gene in Mendelian diabetes. *HNF1A* also carries loss- or gain-of-function coding variants that respectively predispose to or protect against polygenic T2D. The mechanisms underlying HNF1A-deficient diabetes, however, are still unclear. We now demonstrate that diabetes arises from β cell-autonomous defects and identify direct β cell genomic targets of HNF1A. This uncovered a regulatory axis where HNF1A controls transcription of *A1CF*, which orchestrates an RNA splicing program encompassing genes that regulate β cell function. This *HNF1A-A1CF* transcription-splicing axis is suppressed in β cells from T2D individuals, while genetic variants reducing pancreatic islet *A1CF* are associated with increased glycemia and T2D susceptibility. Our findings, therefore, identify a linear hierarchy that coordinates β cell-specific transcription and splicing programs and link this pathway to T2D pathogenesis.

INTRODUCTION

Rare loss-of-function heterozygous *HNF1A* mutations cause maturity-onset diabetes of the young type 3 (MODY3), the most prevalent form of monogenic diabetes.[1] Other rare and common variants that elicit a partial loss of HNF1A function lead to increased susceptibility for polygenic type 2 diabetes (T2D),[2–6] while gain-of-function variants protect against T2D.[7] Furthermore, independent studies have shown HNF1A-dependent transcription defects in islet β cells from individuals with T2D.[8,9]

Despite this pivotal role of HNF1A in the pathogenesis of both monogenic and polygenic forms of diabetes, the cell types where it plays essential roles for normal glucose homeostasis

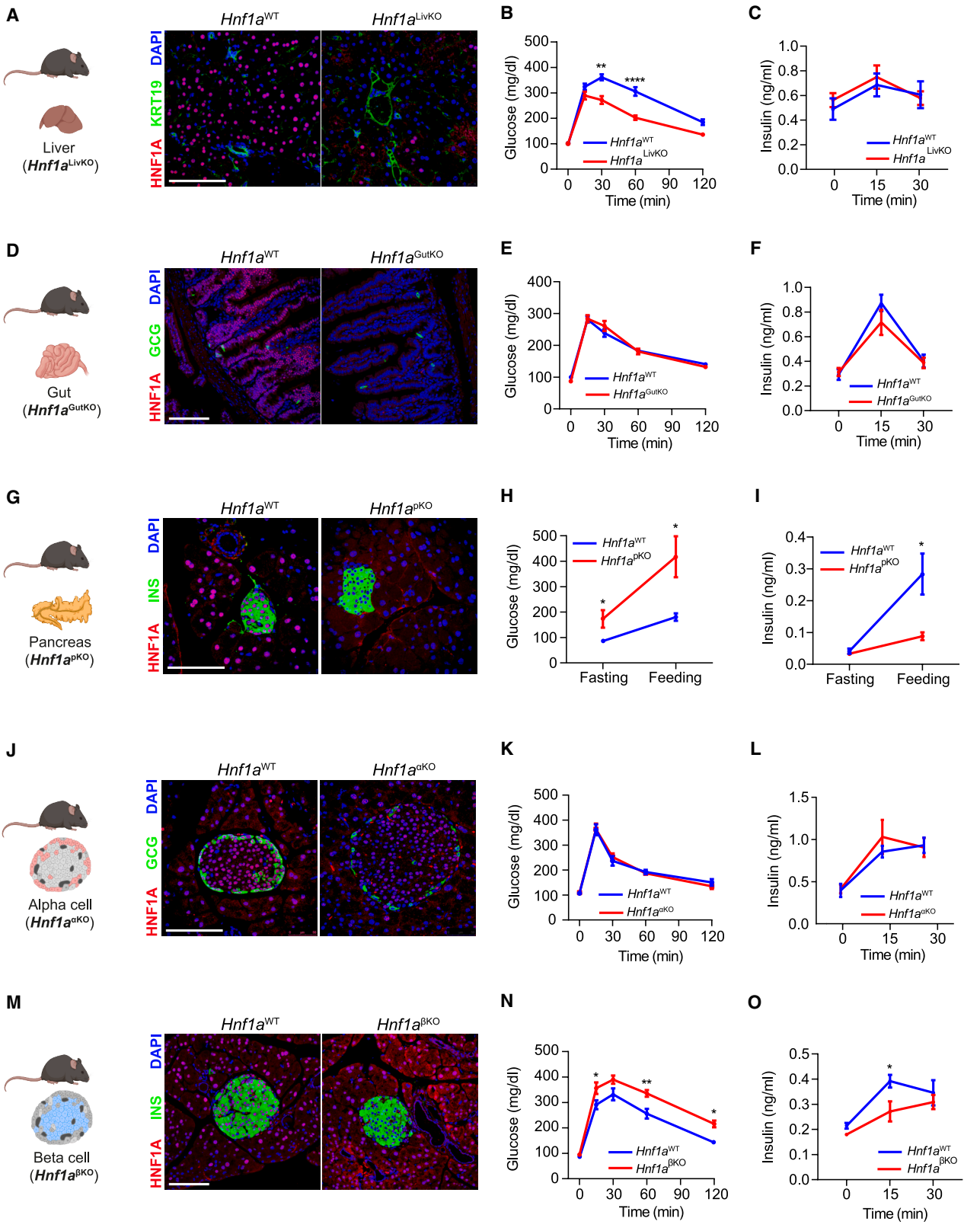

(legend on next page)

remain unclear. Pancreatic β cell dysfunction is prominent in MODY3, as well as in *Hnf1a* homozygous-null mutant mice.[10–13] However, HNF1A controls tissue-specific transcriptional programs in differentiated hepatocytes, kidney and gut cells, and pancreatic acinar and islet cells.[14–18] All of these cell types influence glucose homeostasis and can indirectly affect β cell function.[19–24] Thus, whether HNF1A-deficient diabetes reflects a β cell-autonomous defect is still unknown.

In addition, the molecular mechanisms underlying HNF1A-deficient diabetes are not well understood. Several cellular defects have been documented in *HNF1A* mutant β cells, including defective glucose uptake,[25] glycolytic signaling,[26] or mitochondrial respiration,[27] as well as inconsistent findings regarding abnormal calcium signaling.[28,29] However, these cellular phenotypes have not been unambiguously linked to direct targets of HNF1A, and their relative physiological impact remains unclear.

We now demonstrate that HNF1A-deficient diabetes arises primarily from defective HNF1A function in pancreatic β cells, rather than other HNF1A-expressing cell types. We further identify an evolutionarily conserved β cell transcription program regulated by HNF1A and show that the *A1CF* gene—encoding APOBEC1 complementation factor—is a prominent HNF1A-dependent target. We demonstrate that *A1CF* controls a previously unrecognized β cell splicing program and use single-cell genomics and human genetics to link this pathway to the molecular pathophysiology of T2D. These findings, therefore, uncover a hierarchical mechanism that coordinates β cell transcription and splicing, shedding light on how these two gene regulatory layers can interact to control cell-specific expression.[30,31] We propose that this β cell molecular pathway could be leveraged for therapeutic targeting.

RESULTS

HNF1A-deficient diabetes is a consequence of a β cell-autonomous function

To systematically examine the cell types in which HNF1A is essential to maintain glucose homeostasis, we used lineage-specific mouse Cre lines and a *loxP*-flanked *Hnf1a* exon 2 allele (Figure S1A)[16] to delete *Hnf1a* in liver, gut, or pancreatic lineages.

Hepatocytes have critical glucose homeostatic functions and can indirectly influence β cell function or mass.[22–24] Using a liver-specific Cre line (*Albafp*-Cre, hereafter *Alb*-Cre[32]) (Figure 1A), we inactivated *Hnf1a* in hepatocytes (*Hnf1a*^{LivKO}) and observed that adult male *Hnf1a*^{LivKO} mice recapitulated abnormalities described in germline *Hnf1a*$^{-/-}$ mice,[15] including reduced body weight and fat mass, as well as fatty liver (Figures S1B–S1F). The reduced growth and adiposity in *Hnf1a*$^{-/-}$ mice have been ascribed to decreased liver *Igf1* expression,[10] and our findings confirm that this manifestation reflects a liver-specific HNF1A function. Contrasting with *Hnf1a*$^{-/-}$ mice, however, *Hnf1a*^{LivKO} mice did not exhibit hyperglycemia and instead showed improved intraperitoneal (i.p.) glucose tolerance (272 ± 15 mg/dL vs. 361 ± 12 mg/dL in Cre-only expressing littermates at 30′, $p < 0.0002$, t test) (Figures 1B and 1C), potentially due to the insulin-sensitizing effects of decreased adiposity or to the abnormalities in liver glucose metabolism reported in *Hnf1a* germline mutant mice.[33] Liver HNF1A deficiency, therefore, does not contribute to hyperglycemia observed in *Hnf1a* germline mutants.

Gut cells also have major glucose homeostatic functions related to the gluconeogenic capacity of enterocytes and the enteroendocrine production of incretin hormones that regulate β cell function and mass.[19–21] Using *Vil1*-Cre,[34] we excised *Hnf1a* in intestinal epithelial cells, including GLP1-producing cells (*Hnf1a*^{GutKO}) (Figure 1D). *Hnf1a*^{GutKO} mice did not differ in weight, fasting glycemia, oral glucose tolerance, or insulin responses at 16 weeks when compared with Cre-only expressing littermates (Figures 1E, 1F, and S1G). Thus, HNF1A deficiency in the gut does not recapitulate the diabetic phenotype of *Hnf1a*$^{-/-}$ mice.

To inactivate *Hnf1a* in pancreatic cells, we first used *Pdx1*-Cre, which is active in precursors of all pancreatic epithelial cells (*Hnf1a*^{pKO})[35] (Figure 1G). *Hnf1a*^{pKO} displayed hyperglycemia at weaning (Figure S1H), and at 13 weeks showed fasting and post-prandial hyperglycemia (405 ± 67 mg/dL), with decreased fed plasma insulin (0.09 ± 0.01 vs. 0.28 ± 0.06 ng/mL in Cre-only expressing littermates, $p = 0.019$, t test) (Figures 1H and 1I). The pancreas of *Hnf1a*^{pKO} mice showed unchanged morphology except for fatty infiltration patches in some mice, and there were no significant differences in the relative β cell area (β cell/pancreas area fraction 0.54 ± 0.1 vs. 0.58 ± 0.08 in littermates, $p = 0.77$, t test), suggesting that diabetes in this model was

Figure 1. HNF1A-dependent diabetes requires gene ablation in β cells

(A) Immunofluorescence of HNF1A (red) in adult *Hnf1a*^{LivKO} and control hepatocytes. KRT19 (green) marks biliary duct cells.

(B and C) 13-week-old *Hnf1a*^{LivKO} mice showed improved i.p. glucose tolerance (B) ($n = 14$ controls, 19 *Hnf1a*^{LivKO}) and no significant insulin changes after glucose challenge (C) ($n = 6$ controls, 7 *Hnf1a*^{LivKO}).

(D) Depletion of HNF1A (red) in *Hnf1a*^{GutKO} gut cells, including GLP1 enteroendocrine cells (GCG, green).

(E and F) Oral glucose gavage in 16-week-old *Hnf1a*^{GutKO} mice showing no differences in glucose tolerance (E) ($n = 23$ *Hnf1a*^{WT} and 14 *Hnf1a*^{GutKO} mice) or insulin secretion (F) ($n = 6$ controls and 7 *Hnf1a*^{GutKO}).

(G) Depletion of HNF1A (red) in pancreas from adult pancreas-specific (*Hnf1a*^{pKO}) mice. Insulin is shown in green.

(H and I) 13-week-old *Hnf1a*^{pKO} mice show hyperglycemia upon fasting and 1 h after re-feeding (H) ($n = 5$ controls, 5 *Hnf1a*^{pKO}) and decreased post-prandial insulin secretion (I) ($n = 7$ controls, 6 *Hnf1a*^{pKO}).

(J) Immunofluorescence of 12-week-old *Hnf1a*^{αKO}, 4 weeks after tamoxifen induction, showing HNF1A (red) excision in α cells (GCG, green).

(K and L) i.p. glucose tolerance (K) ($n = 7$ controls, 8 *Hnf1a*^{αKO}) and insulin secretion (L) ($n = 6$ controls, 7 *Hnf1a*^{αKO}) 2 months after tamoxifen treatment.

(M) Immunofluorescence of HNF1A (red) in β cells (green) in adult *Hnf1a*^{βKO} mice.

(N and O) i.p. glucose tolerance (N) ($n = 8$ controls, 12 *Hnf1a*^{βKO}) and insulin secretion (O) ($n = 6$ controls, 5 *Hnf1a*^{βKO}) in *Hnf1a*^{βKO} mice.

For (A), (D), (G), and (M), Cre-expressing littermates without *LoxP* alleles were used as controls. For (J), treated *LoxP* littermates without Cre were used as controls. Student's t test was used in (C), (F), (I), (L), and (O), and two-way ANOVA with Bonferroni's for (B), (E), (H), (K), and (N). *$p < 0.05$, **$p < 0.01$, ****$p < 0.0001$. Scale bars, 100 μm. Error bars represent means ± SEM.

See also Figure S1.

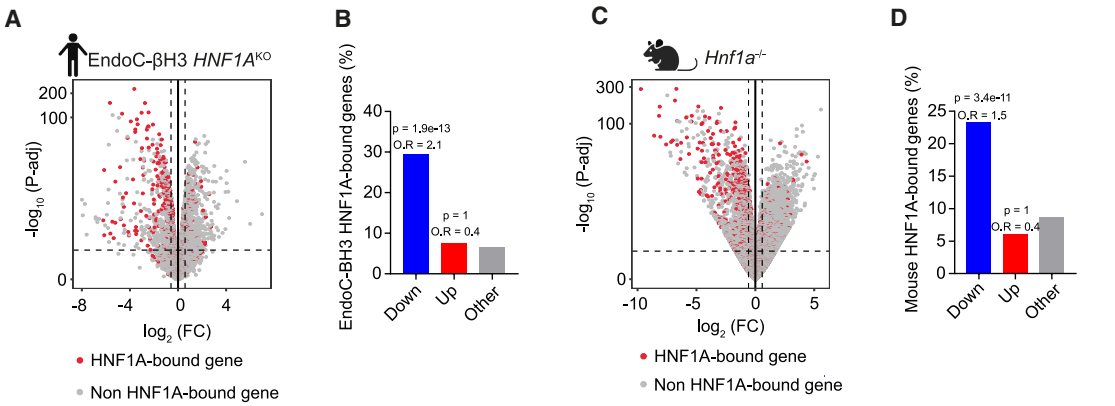

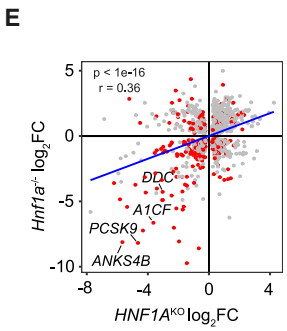

F Top human HNF1A-bound downregulated genes ranked and orthologues

	Human		Mouse	
Gene	log_2FC	Adj p.val	log_2FC	Adj p.val
A1CF	-3.64	5.9e-227	-6.64	2.6e-109
ANKS4B	-5.57	2.6e-152	-8.12	1.5e-167
FGFR4	-2.75	1.1e-151	-1.20	2.9e-05
DDC	-3.04	6.9e-115	-4.28	3.7e-125
PCSK9	-4.66	5.6e-112	-8.18	1.8e-127
AFF2	-5.45	1.6e-107	-1.54	1.3e-19
PRR15L	-3.42	2.6e-95	-1.09	0.007
RBM47	-2.09	5.1e-82	-1.38	3.9e-13
PGM5	-3.55	2.8e-71	-1.30	0.043
GC	-1.57	3.6e-62	-3.71	7.0e-55

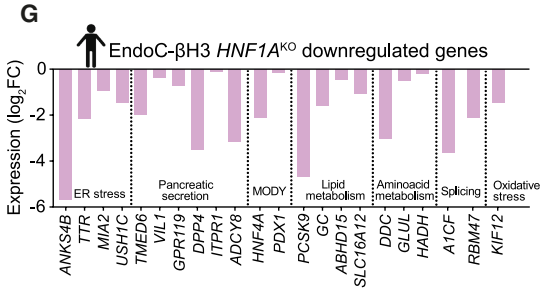

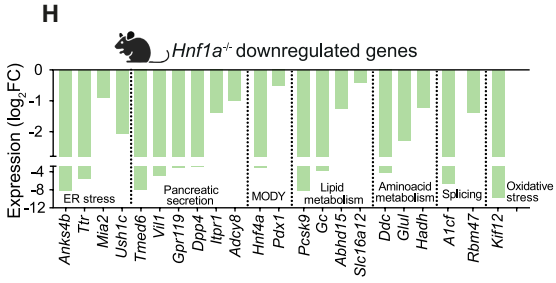

I

EndoC-βH3 *HNF1A*^{KO} Functional annotation

Annotation	Adj p.val
RNA binding	2.5e-13
rRNA binding	7.3e-05
Protein dimerization activity	3.3e-04
mRNA 5´-UTR binding	0.008

Hnf1a$^{-/-}$ Functional annotation

Annotation	Adj p.val
Oxidative phosphorylation	4.1e-23
Protein processing in ER	6.0e-16
Amino Acid metabolism	3.0e-05
RNA Binding	0.04

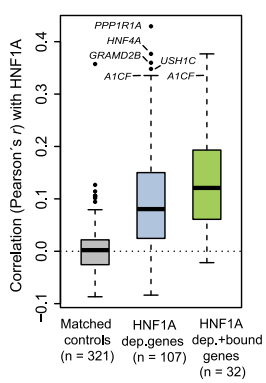

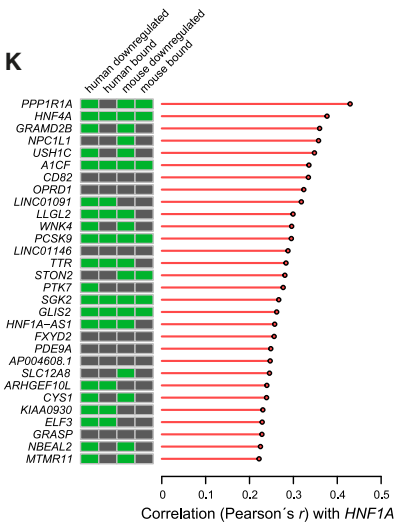

(legend on next page)

primarily caused by β cell dysfunction rather than decreased β cell number (Figures S1I and S1J).

Pancreatic α cells exert paracrine regulation of β cells,[36,37] while MODY3 patients have abnormal glucagon responses to hyperglycemic stimuli.[38,39] We thus used an α cell-specific inducible Cre strain[40] (*Gcg*-Cre^{ERT2}) to inactivate *Hnf1a* perinatally in α cells (hereafter *Hnf1a*$^{\alpha KO}$ mice) (Figure 1J). By 12 weeks, glycemia and insulin after an oral glucose challenge were indistinguishable from tamoxifen-treated Cre-negative littermates (Figures 1K and 1L). However, *Hnf1a*$^{\alpha KO}$ mice showed decreased glucagon responses to insulin-induced hypoglycemia *in vivo*, as well as to low glucose and arginine *in vitro* (Figures S1K–S1M). Thus, α cell *Hnf1a* deficiency does not cause diabetes yet may interfere with counter-regulatory hormonal responses.

Finally, we used an *Ins1*-Cre knockin allele[41] that inactivated *Hnf1a* in β cells gradually after their formation during late gestation, achieving nearly complete *Hnf1a* ablation in adult β cells (*Hnf1a*$^{\beta KO}$) (Figures 1M and S1N). *Hnf1a*$^{\beta KO}$ mice displayed hyperglycemia at weaning (Figure S1O), while 16-week-old *Hnf1a*$^{\beta KO}$ mice showed i.p. glucose intolerance (60 min glucose 336 ± 13 vs. 256 ± 19 mg/dL in Cre-only littermates, $p = 0.005$, ANOVA) and reduced insulin responses (insulin at 15 min 0.04 ± 0.03 vs. 0.27 ± 0.04 ng/mL in controls, $p = 0.049$, t test) (Figures 1N and 1O). Thus, β cell-specific *Hnf1a* inactivation recapitulates hyperglycemia observed in germline mutants, indicating that β cell-autonomous functions of HNF1A are critical for diabetes.

HNF1A regulates a conserved transcriptional program in mouse and human β cells

We next investigated the molecular function of HNF1A in β cells. Given that mouse homozygous and human heterozygous *HNF1A* mutations both cause diabetes, we sought to identify conserved HNF1A-dependent target genes in mouse and human β cells. To this end, we examined human EndoC-βH3 β cells[42] carrying biallelic *HNF1A* deletions and adult *Hnf1a*$^{-/-}$ mouse islets.[10] As expected from previous studies of HNF1A-deficient islet cells,[14,27,43,44] these two models showed profound transcriptional changes (Figures 2A and 2C; Table S3). To define direct effects, we performed chromatin immunoprecipitation sequencing (ChIP-seq) for HNF1A in human EndoC-βH3 and mouse MIN6 β cells (Figures S2A–S2C). We found that HNF1A-bound genes were enriched in genes downregulated in human and mouse mutant models ($p = 1.9 \times 10^{-13}$, $p = 3.4 \times 10^{-11}$, respectively) (Figures 2A–2D), consistent with a primary role of HNF1A as a transcriptional activator in pancreatic β cells.[14]

We found a significant overlap of downregulated ortholog genes in human and mouse HNF1A-deficient models (odds ratio = 4.1, Fisher's $p = 3.9 \times 10^{-33}$) (Figure S2D). Furthermore, direct target genes often showed evolutionarily conserved downregulation and rarely conserved upregulation (Figures 2E and 2F). We thus defined a core set of 129 orthologous genes downregulated in human and mouse models (Figure S2D; Table S3). Many of these ortholog pairs encode for potentially relevant β cell functions, such as endoplasmic reticulum (ER) stress, oxidative stress, lipid metabolism, and RNA splicing (Figures 2G and 2H). Notably, RNA binding was among the most enriched annotations among genes downregulated in both species (Figure 2I; Table S3).

We also investigated HNF1A-dependent regulation in native human β cells. We reasoned that *HNF1A* mRNA variation across single β cells should lead to correlated expression of HNF1A-regulated transcripts and examined this in human β cell transcriptomes from the ESPACE Pancreas Human Cell Atlas consortium. We focused on the 107 conserved HNF1A-dependent genes expressed in >5% of cells and calculated pairwise correlations with *HNF1A* mRNA across β cells. The 107 genes showed markedly higher correlations compared with expression-matched control genes (mean $r = 0.101$ [0.081–0.121, 95% confidence interval (CI)] vs. 0.001 [−0.003–0.005]; $p = 1.1 \times 10^{-16}$). HNF1A-dependent genes that were HNF1A-bound in both species showed even higher correlations ($r = 0.133$ [0.096–0.169]; $p = 2.2 \times 10^{-8}$) (Figure 2J). Remarkably, many of the genes showing the strongest downregulation in *HNF1A* mutants showed the highest correlation values in primary β cells, including known HNF1A targets such as *HNF4A*[18] (ranking 2nd out of 18,242 genes), *HASTER*[45] (*HNF1A-AS1*, 19th), and *A1CF* (6th) (Figure 2K; Table S4). Co-expression analysis, therefore, supported that HNF1A regulates the same conserved gene program in native human β cells. In sum, these findings reveal a conserved transcription program that is controlled by HNF1A in mouse and human β cells and provide a resource to understand the molecular mechanisms underlying HNF1A-deficient diabetes.

HNF1A deficiency leads to reduced expression of RBP genes

Transcripts encoding RNA-binding proteins (RBPs) were enriched among downregulated genes (Figures 2F–2I), including

Figure 2. HNF1A regulates a conserved transcriptional program in mouse and human β cells

(A and C) Differential gene expression in (A) human EndoC-βH3 *HNF1A*^{KO} vs. control cells ($n = 3$ replicates/group) and (C) mouse *Hnf1a*$^{-/-}$ vs. wild-type islets ($n = 4$ replicates/group), highlighting HNF1A-bound genes in red. Dashed lines depict $\log_2$ fold-change ($\log_2$FC) > 0.585 and adjusted $p < 0.05$, used for calling differential expression.

(B and D) HNF1A binding was enriched in downregulated, but not upregulated, genes in EndoC-βH3 *HNF1A*^{KO} cells and *Hnf1a*$^{-/-}$ islets. OR, odds ratio relative to all active genes; *p* values, Fisher's exact test.

(E) $\log_2$FC values of differentially expressed orthologs in human *HNF1A*^{KO} vs. mouse *Hnf1a*$^{-/-}$, with HNF1A-bound in red, and Pearson correlation coefficient with *p* value.

(F) Top 10 differentially expressed genes ranked by adjusted *p* value in *HNF1A*^{KO} cells. All showed downregulation in *Hnf1a*$^{-/-}$ islets.

(G and H) $\log_2$FC for downregulated genes from selected annotations in *HNF1A*^{KO} cells (G) and *Hnf1a*$^{-/-}$ islets (H).

(I) Significant annotation terms for downregulated genes.

(J) Normalized human islet β cell single-cell VASA-seq expression counts were used to calculate Pearson's coefficients of *HNF1A* mRNA vs. 107 conserved HNF1A-dependent transcripts across all β cells (middle bar) vs. expression-matched control genes (left bar) or conserved HNF1A-dependent genes bound by HNF1A (right bar). Error bars represent 95% CI.

(K) Top 30 *HNF1A* mRNA-correlated genes in human β cells. Genes showing downregulation in *HNF1A* mutants or HNF1A binding are highlighted in green.

See also Figure S2.

five RBP orthologs downregulated in mouse and human knockouts (Figures 3A–3C). In particular, *A1CF*, encoding APOBEC1 complementation factor, showed very low expression in mouse and human *HNF1A* knockouts (Figures 2F, 3B, and 3C) and was among genes showing the highest correlations with *HNF1A* mRNA in native β cells ($r_P = 0.34$, $p = 10^{-42}$) (Figures 2J and 2K). The mouse and human *A1CF* genes were bound by HNF1A at multiple sites, indicating direct regulation (Figures 3D, 3E, and S2E). Immunolocalization studies showed that A1CF is expressed in most mouse islet cells, with markedly reduced expression in *Hnf1a* mutants (Figure 3F).

A1CF was originally described as a cofactor in the APOBEC1 RNA editing complex but was later found to be dispensable for APOBEC1-dependent RNA editing activity and more recently shown to be a direct regulator of alternative splicing of liver transcripts encoding fructose and glycerol metabolism enzymes.[46–49] Interestingly, *A1CF* mRNA is exclusively expressed in tissues expressing high *HNF1A* mRNA, namely in the liver, stomach, gut, kidney, and pancreas (Figure 3G), and *A1cf* mRNA also showed partially decreased expression in liver and gut from tissue-specific *Hnf1a* mutants (Figures S2F and S2G). These findings, therefore, demonstrated that HNF1A is an essential regulator of *A1CF* in β cells and suggested that HNF1A could indirectly influence cell-specific RNA processing.

HNF1A controls an alternative splicing program in mouse and human β cells

To study if HNF1A regulation of A1CF impacts β cell RNA splicing, we analyzed RNA sequencing (RNA-seq) data from mouse and human HNF1A-deficient models, using replicate multivariate analysis of transcript splicing (rMATS).[50] This revealed that HNF1A deficiency not only causes major transcript changes in β cells but also profoundly alters RNA splicing (Figures 4A–4D). We identified 864 and 2,362 differential splicing events in HNF1A-deficient mouse islets and human EndoC-βH3 cells, respectively, ∼60%–70% of which were exon inclusion or skipping events (Figures 4B and 4D). Importantly, most differentially spliced genes did not show differential mRNA expression in the same models (Figures S3A and S3B).

To assess the conservation of the HNF1A-dependent RNA splicing program, we calculated delta percent spliced-in (ΔPsi) values to measure the percentage of transcripts that include differentially spliced exons in mutant vs. control conditions. This revealed that human and mouse HNF1A-dependent splicing changes were significantly correlated ($r = 0.64$; $p < 9.4 \times 10^{-13}$) (Figure 4E). We identified 134 genes showing HNF1A-dependent splicing in orthologous exons in both species (Figure 4F; Table S5). Among the top five genes showing the strongest differential splicing, *SLC7A2* is a cationic amino acid transporter involved in arginine-induced insulin secretion,[37] *SEC31A* is a COPII coat protein that mediates proinsulin processing and vesicle budding from the ER in β cells,[51] and *MYO6* has been implicated in membrane traffic in the secretory pathway[52,53] (Figures 4G–4M; Table S5).

In keeping with reduced *A1CF* mRNA in HNF1A-deficient cells, mutually exclusive differentially spliced events in *HNF1A*^{KO} cells were enriched in A1CF recognition motifs at flanking locations (Figure S3C), while differentially spliced events from *Hnf1a*$^{-/-}$ islets showed significant overlaps with those identified in *A1cf* mutant liver[48] (Figure S3D). Taken together, these observations point to a previously unrecognized role of HNF1A in the regulation of alternative splicing in mouse islets and human β cells, potentially mediated through its direct target A1CF.

A1CF regulates a broad β cell splicing program that is altered in HNF1A deficiency

To further assess whether A1CF underpins HNF1A-mediated splicing, we created *A1CF* null mutant EndoC-βH3 cells by engineering homozygous single-exon deletions. *A1CF*^{KO} cells showed profound alternative splicing changes, with 1,907 differentially spliced events in 1,372 genes (Figures 5A and 5B; Table S5), most of which did not show differential expression (Figure S4A). As observed for *HNF1A*^{KO} cells, most differentially spliced events were exon skipping or inclusion events (Figures 5B and 5C), and A1CF recognition motifs were enriched ∼200 bp downstream of differentially spliced mutually exclusive exons[54] (Figure S4B).

The A1CF-dependent β cell splicing program was prominently enriched in genes involved in intracellular protein targeting and degradation processes, including annotations such as *trans*-Golgi network, COPII-mediated vesicle transport, vesicle targeting, clathrin-mediated endocytosis, Rho GTPases, ER or membrane trafficking, as well as other functions related to cilium, DNA repair, and RNA splicing (Figure 5D; Table S6). Thus, A1CF regulates a distinct β cell splicing program.

The *A1CF* and *HNF1A* mutant splicing phenotypes were remarkably similar. 45% of genes with altered splicing in *A1CF*^{KO} cells were significantly mis-spliced in *HNF1A*^{KO} cells (odds ratio = 12.9; $p = 2.6 \times 10^{-314}$), while 38% of differentially spliced genes in *HNF1A*^{KO} cells showed abnormal splicing in *A1CF*^{KO} cells at false discovery rate (FDR) < 0.05, and 59% at $p < 0.05$ (Figure 5E; see also Figure S4C). Crucially, differentially spliced events in *HNF1A*^{KO} cells showed highly correlated ΔPsi values in *A1CF*^{KO} cells ($r = 0.7$, $p < 1 \times 10^{-16}$), indicating that most HNF1A-dependent splicing abnormalities are also A1CF-dependent (Figure 5F).

Genes showing differential splicing in *HNF1A*^{KO} and *A1CF*^{KO} cells expectedly showed shared enrichment of functional annotations (Figure S4D; Table S6). Notably, numerous genes with documented β cell functions were differentially spliced in both *HNF1A*^{KO} and *A1CF*^{KO} cells. For example, *SLC7A2* showed differential mutually exclusive splicing of exons 7 and 8, with decreased exon 8 inclusion, in both *HNF1A*^{KO} and *A1CF*^{KO} cells (Figures 5C and 5G–5I). Re-expression of *A1CF* in *A1CF*^{KO} β cells enhanced *SLC7A2* exon 8 expression, confirming that A1CF is a direct effector (Figures 5J and S4E). Likewise, secretory pathway genes *MYO6* and *SEC31A*[51–53] (Figure 5K), as well as numerous other abnormal splicing events in both mutants, occurred in genes with known β cell regulatory functions, including *SIDT2*,[55] *SIRT6*,[56] *ERC1* (ELKS),[57] *MARK2*,[58] *ELAVL4* (HuD),[59] *ACSL4*,[60] *ARHGEF7* (βPix),[61] or *ABCC8* (SUR1)[37] (Tables S5 and S7).

Thus, A1CF controls a broad β cell splicing program that includes many known regulators of β cell function. This splicing program is impaired in *HNF1A*-deficient cells, with a profound reduction in A1CF expression and A1CF-dependent splicing. This indicates that HNF1A regulates β cell splicing, at least in part, through direct control of A1CF.

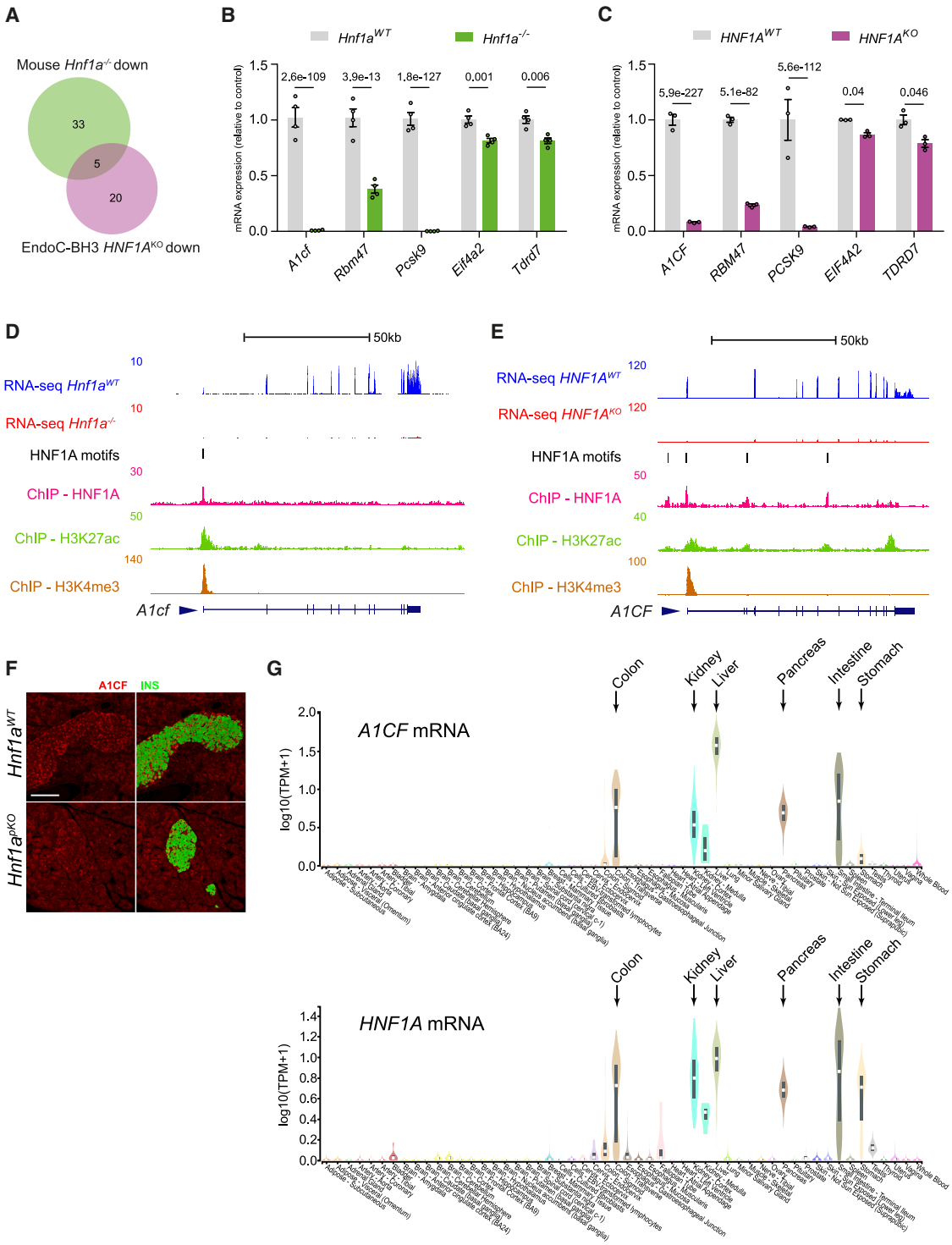

Figure 3. HNF1A directly regulates *A1CF*

(A) HNF1A-bound genes encoding RBPs downregulated in *Hnf1a*$^{-/-}$ islets and *HNF1A*^{KO} cells.

(B and C) RNA-seq expression counts of downregulated RBP genes in *HNF1A*^{KO} cells, *Hnf1a*$^{-/-}$ islets, and controls. Adjusted *p* values were calculated with Benjamini-Hochberg (DESeq). Bar graphs represent means and SEM.

(D and E) RNA-seq counts for *A1CF* in (D) *Hnf1a*$^{-/-}$ and control islets and (E) *HNF1A*^{KO} and control cells, as well as HNF1A, H3K27ac, and H3K4me3 ChIP-seq signals. Vertical lines indicate HNF1A recognition sequence motifs (see also Figure S2).

(F) A1CF (red) and insulin (green) immunofluorescence in *Hnf1a*^{pKO} islets. Scale bar, 100 μm.

(G) Tissue-wide expression of *A1CF* and *HNF1A* mRNAs from GTEx. Arrows highlight tissues with prominent *HNF1A* expression.

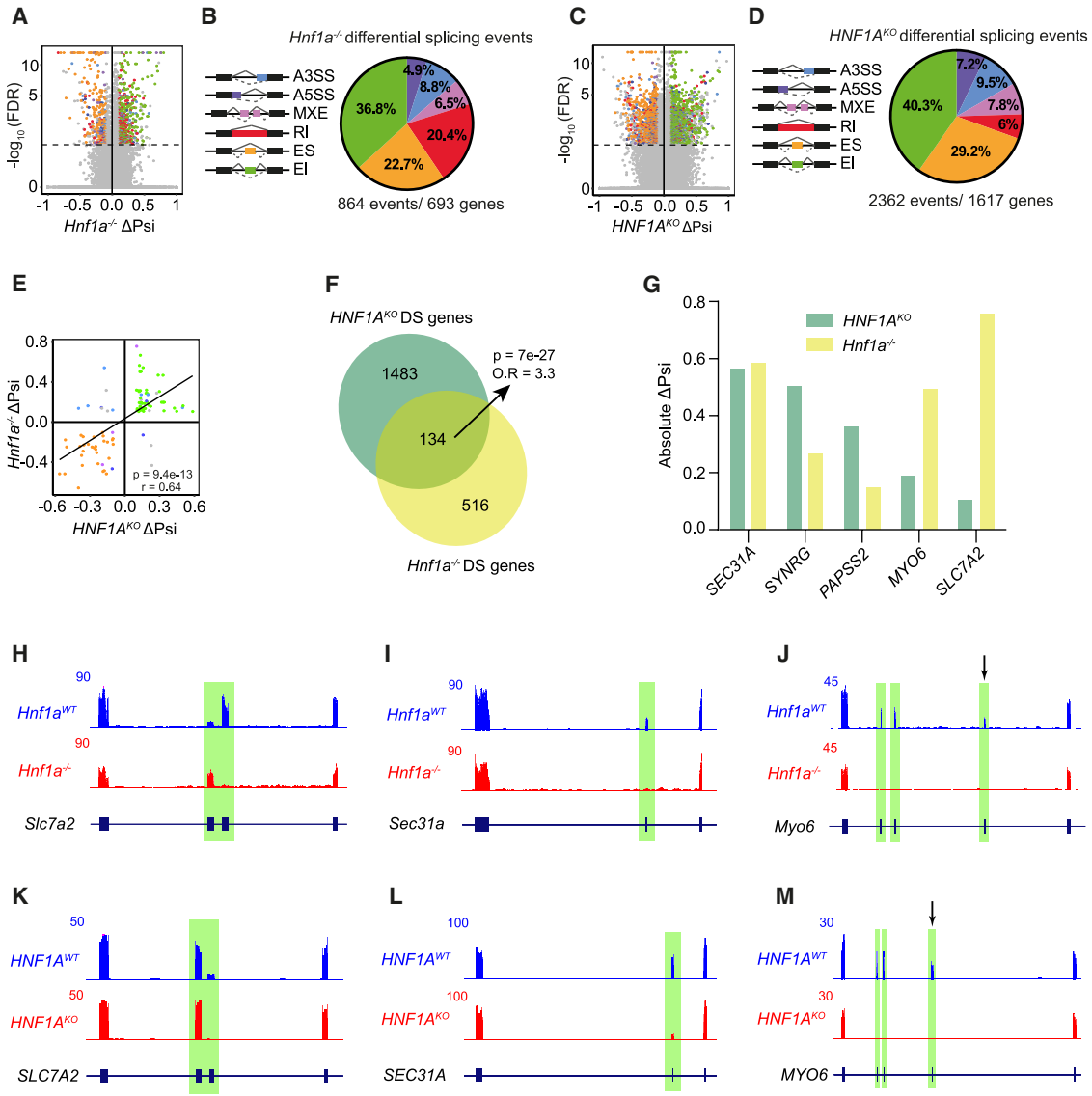

Figure 4. HNF1A regulates AS in mouse and human β cells

(A) Volcano plot showing ΔPsi and $-\log_{10}$ FDR values for *Hnf1a*$^{-/-}$ islets (n = 4 replicates/group).

(B) Differentially spliced (DS) event types in *Hnf1a*$^{-/-}$ islets.

(C) ΔPsi and $-\log_{10}$ FDR values for *HNF1A*^{KO} cells (n = 3 replicates/group).

(D) DS event types in *HNF1A*^{KO} cells. The dashed lines show FDR < 0.05. Negative and positive ΔPsi values are, respectively, skipping and inclusion events. A3SS, alternative 3′ splice site; A5SS, alternative 5′ splice site; MXEs, mutually exclusive exons; RI, retained intron; EI, exon inclusion; ES, exon skipping.

(E) Correlation of ΔPsi between DS events in mouse and human mutants, using the same color code to represent event types, and showing Pearson correlation coefficient and p value.

(F) Overlap between mouse *Hnf1a*$^{-/-}$ and human *HNF1A*^{KO} DS genes with recognizable orthologs, with Fisher's exact test p value. OR, odds ratio relative to all active genes.

(G) Top five DS genes ranked by ΔPsi in *HNF1A*^{KO} cells.

(H–M) Examples of DS exons (highlighted in green) in *Hnf1a*$^{-/-}$ islets (H–J) and *HNF1A*^{KO} cells (K–M). The direction of transcription is from left to right.

See also Figure S3.

A1CF deficiency leads to impaired insulin secretion

To examine the functional impact of the HNF1A- and A1CF-dependent splicing in β cells, we focused on the CAT2 cationic amino acid transporter encoded by *SLC7A2*, which enables the transport of arginine, a potent insulinotropic molecule.[62,63] The differentially spliced *SLC7A2* isoforms in our models have been previously characterized as CAT-2A and CAT-2B, which differ by mutually exclusive inclusion of exons 8 and 7[64] (Figure 6A). The inclusion of exon 8, which is decreased in *HNF1A* and *A1CF* mutants, confers ~3-fold higher arginine transport capacity and lower affinity over the alternative exon 7 isoform[64,65] (Figure 6A) and

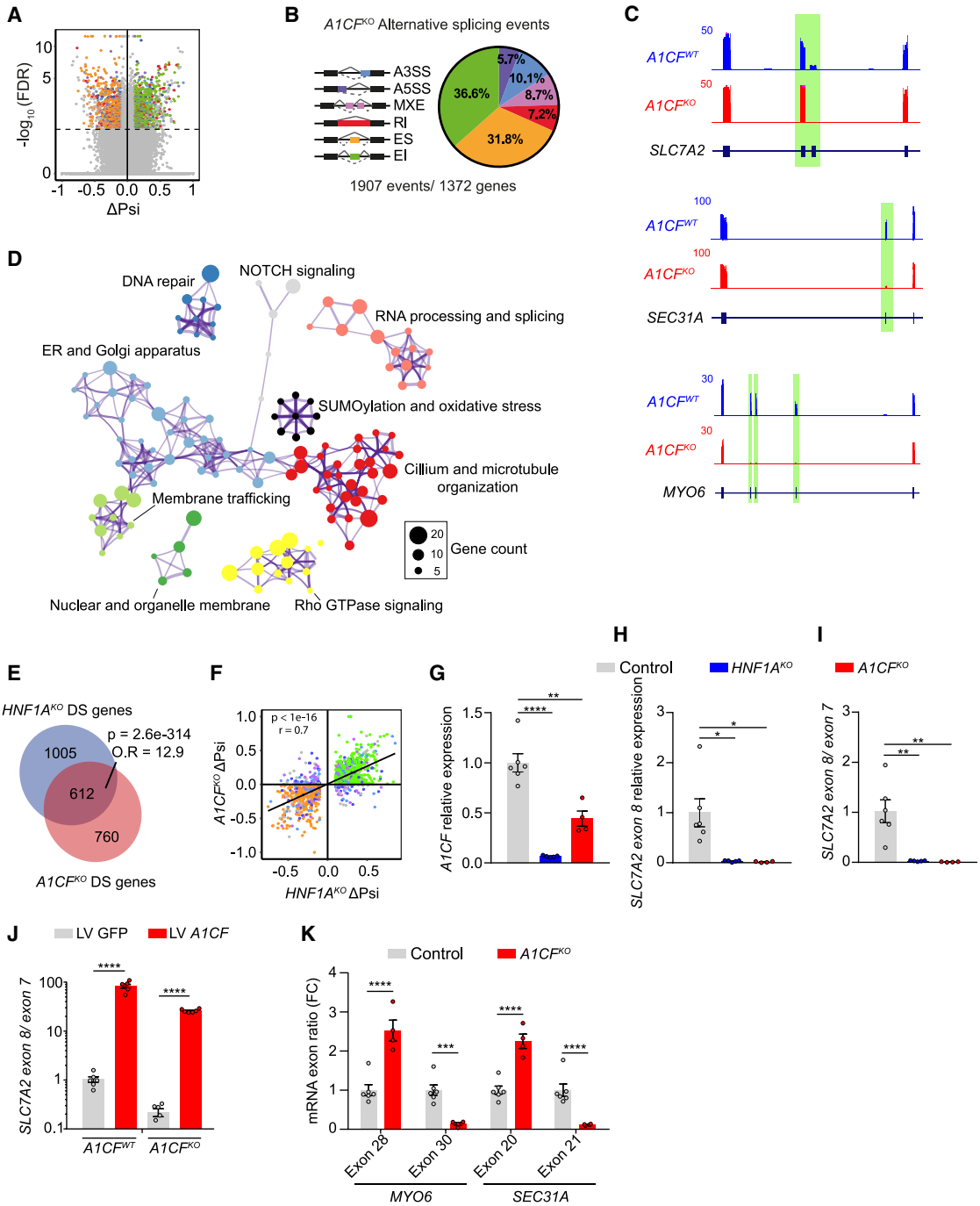

Figure 5. *A1CF* knockouts recapitulate HNF1A-dependent splicing

(A) Volcano plot showing ΔPsi and $-\log_{10}$ FDR values for *A1CF*^{KO} vs. control cells (n = 3 replicates/group). The dashed line shows FDR < 0.05.

(B) Classification of DS events in *A1CF*^{KO} cells. A3SS, alternative 3′ splice site; A5SS, alternative 5′ splice site; MXEs, mutually exclusive exons; RI, retained intron; EI, exon inclusion; ES, exon skipping.

(C) Examples of DS exons, highlighted in green.

(D) Functional annotations enriched in DS genes in *A1CF*^{KO} cells. Circle sizes indicate gene counts in nodes, and colors represent pathways.

(E) Enrichment of shared DS genes in *A1CF*^{KO} and *HNF1A*^{KO} cells. OR, odds ratio relative to all active genes. p value was calculated with Fisher's exact test.

(F) DS events in *HNF1A*^{KO} cells showed highly correlated ΔPsi values in *A1CF*^{KO} cells. Pearson correlation coefficient and p value are shown.

(G) Validation of decreased expression in *HNF1A*^{KO} and *A1CF*^{KO} cells. *A1CF* transcripts are detectable in *A1CF*^{KO} cells because of incomplete nonsense-mediated decay.

(legend continued on next page)

has been suggested to mediate arginine-induced insulin secretion.[63]

To study the impact of *SLC7A2* splicing on arginine responsiveness in EndoC-βH3 cells, we inhibited *A1CF* mRNA using antisense oligonucleotides (ASOs) or directly blocked *SLC7A2* exon 7 or 8 inclusion using splice-switching oligonucleotides (SSOs) (Figures S5A–S5F). Inhibition of *A1CF* mRNA, which inhibited *SLC7A2* exon 8 inclusion, as well as direct blocking of exon 8 inclusion, both led to reduced insulin responses to 10 mM arginine (*A1CF* ASO stimulation index: 1.22 ± 0.13 vs. 2.02 ± 0.21 in controls, $p = 0.004$; *SLC7A2* exon 8 SSO: 1.48 ± 0.1 vs. 2.02 ± 0.21 in controls, $p = 0.03$, t test) (Figures S5G and S5H). Likewise, $A1CF^{KO}$ EndoC-βH3 cells displayed reduced arginine-dependent insulin stimulation (1.47 ± 0.20 vs. 2.84 ± 0.10 in controls, $p < 0.0001$, t test) (Figures 6B and 6C).

We further generated homozygous *A1CF* exon deletions in human embryonic stem cells (hESCs) and differentiated them to glucose-responsive stem-cell-derived islets (SC islets), which expectedly showed decreased *SLC7A2* exon 8 inclusion (Figures 6D–6F) and abnormal *MYO6* and *SEC31A* splicing (Figure S5I). $A1CF^{KO}$ SC islets showed normal insulin content and a robust insulin secretory response to high glucose, whereas 10 mM arginine responsiveness was decreased (arginine/15 mM glucose stimulation index: 2.22 ± 0.15 vs. 2.83 ± 0.2 in controls, $p = 0.02$, t test) (Figures 6G, 6H, and S5J–S5M). Therefore, A1CF deficiency and altered *SLC7A2* splicing cause impaired β cell function with abnormal arginine responsiveness.

Given that HNF1A regulates *A1CF* expression and *SLC7A2* splicing, we examined arginine responses in HNF1A-deficient β cells. We generated homozygous $HNF1A^{KO}$ SC islets (Figures 6I and S5N), which showed profound *A1CF* downregulation, a 90% decrease in *SLC7A2* exon 8/7 ratios (Figures 6J and 6K), and abnormal *MYO6* and *SEC31A* splicing (Figure S5O). $HNF1A^{KO}$ SC islets predictably showed severely impaired secretory responses to glucose and exendin-4, as well as fewer β-like cells and less insulin content (Figures 6I, S5P, and S5Q). This severe β cell impairment can be caused by multiple concomitant HNF1A-dependent molecular defects. We therefore assessed the effects of re-expressing *HNF1A* in $HNF1A^{KO}$ SC islets, which led to increased *A1CF* mRNA, *SLC7A2* exon 8 inclusion, and insulin response to 10 mM arginine (Figures 6L–6N) (insulin area under the curve 242.6 ± 6.21 vs. 185.7 ± 6.09 in controls, $p = 0.0028$). Thus, restoration of HNF1A expression in $HNF1A^{KO}$ SC islets enhanced *SLC7A2* splicing and arginine-induced insulin secretion.

We further examined *Hnf1a* mutant mice, which also showed abnormal *Slc7a2* splicing (Figure 4H). Isolated islets from 4-week-old $Hnf1a^{\beta KO}$ mice still displayed normal glucose-stimulated insulin secretion yet showed decreased arginine stimulation index (1.42 ± 0.15 vs. 1.86 ± 0.06 in controls, $p = 0.038$, t test) (Figures 6O and 6P). $Hnf1a^{iPancKO}$ mice, in which *Hnf1a* was excised in β cells after 8 weeks of age (Figure S5R), did not develop fasting hyperglycemia or major glucose tolerance and insulin secretion changes (glucose/insulin ratio 361.9 ± 31.0 vs. 260.9 ± 48.4 in controls, t test $p = 0.097$) (Figures S5S–S5U) yet displayed impaired glycemic responses after i.p. arginine injection (8% glycemic decrease at 15 min vs. 25% in control mice, $p = 0.001$, t test), without significant changes in insulin levels (Figures 6Q–6S). Furthermore, isolated islets from non-diabetic $Hnf1a^{iPancKO}$ mice showed impaired arginine-dependent electrical activity. Thus, whereas β cells from $Hnf1a^{iPancKO}$ and control mice readily depolarized in response to 100 μM tolbutamide (Figures 6T and 6U), 10 mM L-arginine initiated action potential firing and depolarization in only 20% of $Hnf1a^{iPancKO}$ β cells, in contrast to all control cells ($p < 0.048$, Fisher's exact test) (Figures 6T–6V). Taken together, these experiments showed a prominent impairment of arginine-induced insulin secretion in mouse and human *HNF1A* mutant models (Figure 6A). Our findings have also demonstrated that the splicing factor A1CF regulates β cell function and point to a potential molecular mediator of the HNF1A-deficient secretory phenotype.

A1CF-dependent splicing changes in T2D-associated β cell subpopulations

We next sought evidence that HNF1A influences A1CF-dependent splicing in primary human β cells. Human β cells have been recently shown to be heterogeneous, with transcriptional states that differ by HNF1A activity.[8,9] We reasoned that if HNF1A controls A1CF expression in native human islets, this should lead to increased A1CF-dependent splicing in β cells that have higher HNF1A activity. We therefore analyzed single-cell transcriptomes from the Human Cell Atlas ESPACE consortium generated with VASA-seq, a method that is suited for profiling RNA splicing because it captures full-length transcripts in single cells.[66] Using pooled VASA-seq data from human islet samples from 11 individuals (5 with T2D, 6 without diabetes), we first clustered major cell types, yielding 2,036 β cells (Figure S6A), and defined major β cell clusters (Figure 7A). We then computed for each β cell cluster the expression of 172 HNF1A target genes (bound by HNF1A and downregulated in $HNF1A^{KO}$ cells). This revealed a β cell cluster (#2) with distinctly higher HNF1A activity (Figure 7B). These $HNF1A^{High}$ β cells showed widespread differential splicing relative to all other β cells (Figure S6B), and these changes were enriched in abnormally spliced events from $A1CF^{KO}$ β cells (NES = 1.75 or −1.19, $q = 7.2 \times 10^{-5}$ or 0.12 for splicing events showing decreased or increased inclusion in $A1CF^{KO}$ cells, respectively) (Figures 7C and S6C). Therefore, major β cell states differ not only by *HNF1A* activity but also by differences in A1CF-dependent splicing. These results are consistent with HNF1A-dependent regulation of A1CF-dependent splicing in native human β cells.

To assess the implications of this finding for T2D, we focused on β cell states previously associated with T2D. A recent study used machine learning to distinguish β1 and β2 cell states that are depleted or enriched in islet donors with T2D and exhibit

(H and I) Decreased *SLC7A2* exon 8 and *SLC7A2* exon 8 to exon 7 ratio in both mutant models. $n = 6–4$.
(J) Restoration of *SLC7A2* exon 8 to exon 7 expression after *A1CF* overexpression in $A1CF^{KO}$ cells. $n = 6$ lentiviral transduction replicates.
(K) $A1CF^{KO}$ cells show DS in genes with β cell-relevant functions. $n = 4–6$. Student's t test was used on (G)–(K) $^{*}p < 0.05$, $^{**}p < 0.01$, $^{****}p < 0.0001$. Bar graphs represent means ± SEM.
See also Figure S4.

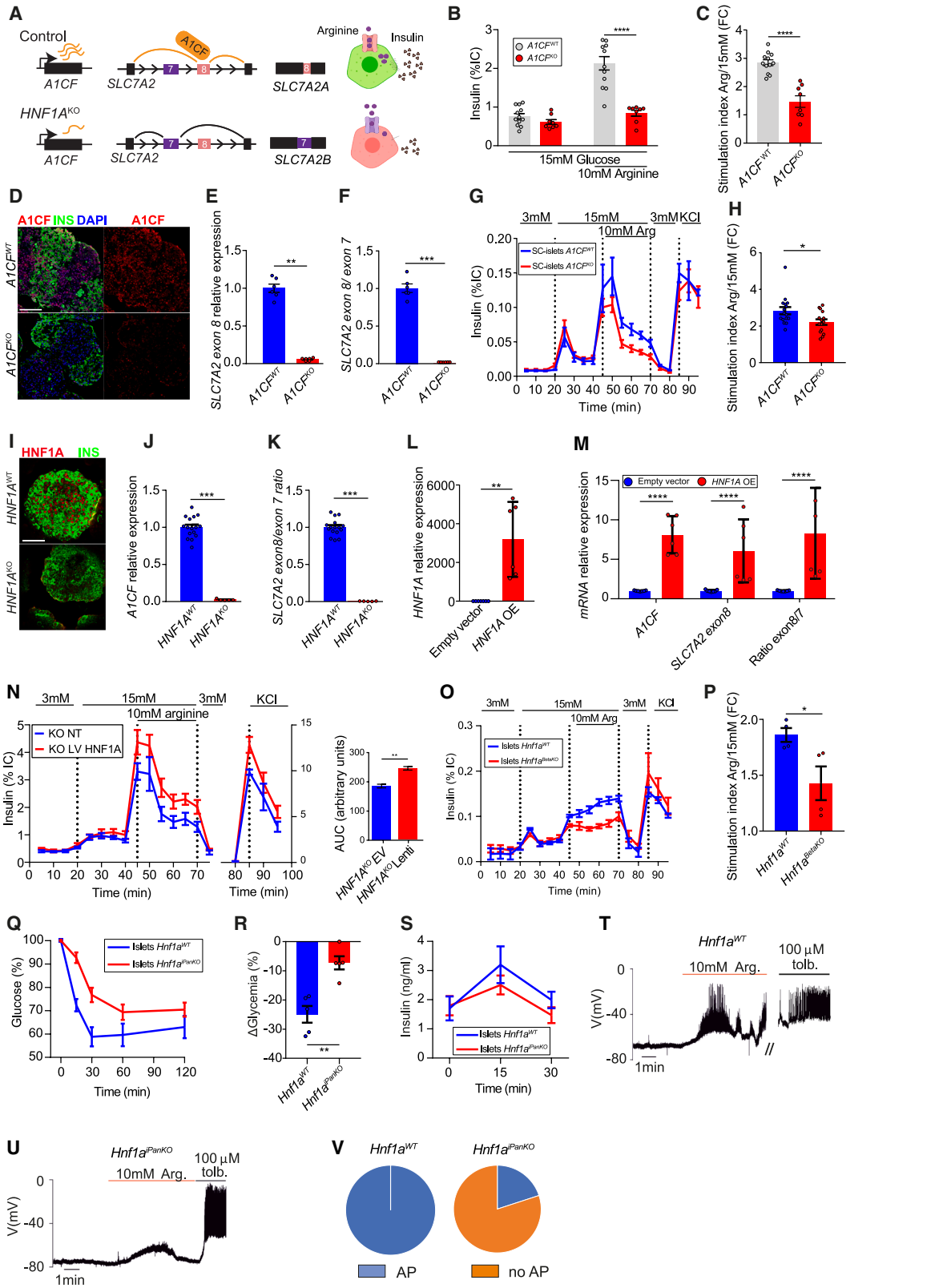

Figure 6. Abnormal A1CF-dependent splicing leads to impaired insulin secretion

(A) HNF1A-dependent regulation of A1CF drives increased inclusion of *SLC7A2* exon 8, which confers high-capacity arginine transport.

(B and C) *A1CF*^{KO} cells show impaired insulin response to arginine in static incubations. *n* = 8–12, 2 independent experiments. IC, insulin content.

(legend continued on next page)

either increased or decreased HNF1A activity, respectively.[9] We analyzed β1 and β2 gene marker sets in our data and observed that HNF1A^{High} β cells had a distinct β1 gene signature, two other clusters had prominent β2 signature, while the remaining cells had low expression of both gene sets (Figures 7A and 7B). β2 cells, which had low HNF1A activity, were increased in individual donors with T2D, while β1 (HNF1A^{High}) cells were decreased (Figure 7D), and the β2/β1 cell ratio was ∼8-fold higher in T2D vs. non-T2D donors ($p = 4 \times 10^{-3}$; Wilcoxon test) (Figure 7E). This new dataset, therefore, confirmed that T2D entails an unambiguous inversion of β1 and β2 cell states.

We next examined splicing specifically in T2D-associated β cell states and found that splicing events showing decreased inclusion in *A1CF*^{KO} cells were also decreased in β2 cells, whereas those showing increased inclusion in *A1CF*^{KO} cells were increased in β2 cells compared with β1 cells; thus, splicing events showing negative regulation in *A1CF*^{KO} cells had a β2 vs. β1 ΔPsi value of −0.192 [−0.248, −0.037] 95% CI, whereas events showing positive regulation in *A1CF*^{KO} cells had a value of 0.071 [−0.072, 0.130] 95% CI ($p = 0.01$, Wilcoxon test) (Figure 7F). For example, the *SLC7A2* exon 8 isoform, which was decreased in *HNF1A*^{KO} and *A1CF*^{KO} cells and known to mediate high-capacity arginine transport, was suppressed in T2D-associated β2 cells (Figure 7G). Likewise, T2D-associated β2 cells recapitulated *HNF1A*^{KO} and *A1CF*^{KO} differential splicing events in *SIRT6* and *SEC31A* (Figure S6D). Taken together, these results reveal that β cell state alterations in T2D entail not only differences in gene expression but also abnormal A1CF-dependent RNA splicing.

Variation at *A1CF* shows association with T2D and glycemic traits

To further investigate the *in vivo* impact of *A1CF* on human glucose homeostasis, we asked whether genetic variation at *A1CF* influences glycemic traits and T2D in recent large-scale meta-analyses.[67,68] This showed that intragenic *A1CF* variants are associated with random glucose levels ($p = 7.3 \times 10^{-12}$) and T2D risk ($p = 2.8 \times 10^{-9}$) (Figure 7H). Fine-mapped genetic signals contained candidate causal variants located in human pancreatic islet enhancers that are connected by chromatin interaction maps to the *A1CF* promoter[69] (Figure 7I). Despite their proximity, the glucose and T2D association signals could be genetically independent, based on low linkage disequilibrium (LD) ($r^2 = 0.18$, $D' = 0.46$) and poor genetic colocalization (*COLOC* PP4 < 0.1). To investigate whether *A1CF* is a plausible effector gene for these associations, we carried out a transcriptome-wide association (TWAS) analysis[70] in ∼400 human islet RNA-seq samples[71] and found a significant association between islet *A1CF* expression and random glucose (Figure S6E; Table S7). Accordingly, the lead *A1CF* TWAS variant, rs61856594, elicits a human islet *A1CF* eQTL ($p = 4.2 \times 10^{-8}$) that shows genetic colocalization with the random glucose association (COLOC PP = 0.99) (Figures 7J and 7K). Likewise, the lead T2D variant, rs12570156, showed associations at nominal significance with an islet *A1CF* eQTL in various datasets ($p = 2.4 \times 10^{-3}$, 2.1×10^{-3}, and 4.1×10^{-4})[71–73] and an eQTL in whole pancreas ($p = 1 \times 10^{-5}$, Genotype-Tissue Expression [GTEx] v8)[74] (Figure 7L).

Further analysis of the random glucose (rs61856594) and T2D (rs12570156) lead variants showed that alleles increasing *A1CF* gene expression steered lower random glucose levels[68]; lowered T2D risk[67]; improved β cell function, glucose tolerance, and acute insulin response (BIGTT-AIR[75]); and were associated with increased birth weight[76] and pancreas volume[77]—two traits for which Mendelian and polygenic studies have shown strong dependence on insulin secretion[78–81] (Figure 7M; Table S8). Consistent with *A1CF* expression in other tissues, the same alleles had pleiotropic effects, notably increased hepatic levels of the enzyme gamma glutamyl transferase[82] (Figure 7M; Table S8), while a low-frequency *A1CF* missense variant is associated with hypertriglyceridemia.[83] Thus, consistent with the predictions from our functional studies, human genetic evidence supports that increased islet *A1CF* expression improves β cell function and glucose homeostasis and limits T2D predisposition.

DISCUSSION

We have shown that HNF1A-deficient diabetes stems from a cell-autonomous function of HNF1A in β cells and identified the direct transcriptional targets of HNF1A in this cell type. Our study revealed that *HNF1A* is an indispensable regulator of *A1CF* in β cells, forming a regulatory hierarchy that orchestrates a β cell

(D) Immunofluorescence for insulin (green) and A1CF (red) in stage 7 *A1CF*^{KO} SC islets.
(E and F) Reduced *SLC7A2* exon 8 and exon 8/7 ratio in *A1CF*^{KO} SC islets, $n = 6$.
(G and H) Representative perifusion experiment showing impaired arginine-induced insulin secretion in *A1CF*^{KO} SC islets. The arginine/15 mM glucose stimulation index in (H) was calculated from $n = 15–16$ replicates (4 independent experiments).
(I) Immunofluorescence for insulin (green) and HNF1A (red) in stage 7 *HNF1A*^{KO} SC islets.
(J and K) *HNF1A*^{KO} SC islets display reduced *A1CF* mRNA and *SLC7A2* exon 8/7 ratios. $n = 5–16$.
(L and M) *HNF1A*^{KO} SC islets transduced with HNF1A-expressing lentivirus restored exon 8/7 ratios. $n = 6$.
(N) Perifusion experiment showing enhanced arginine-induced insulin secretion in *HNF1A*^{KO} SC islets re-expressing *HNF1A*. $n = 3–4$. Right panels show insulin AUC during arginine responses.
(O and P) Isolated islets from *Hnf1a*$^{\beta KO}$ mice show decreased arginine-stimulated insulin secretion and arginine/15 mM glucose stimulation index. $n = 4$.
(Q–S) *Hnf1a*^{iPanKO} mice show impaired arginine sensitivity. *Hnf1a* was deleted in adult mice without causing glucose intolerance (Figure S5S). *Hnf1a*^{iPanKO} displayed impaired *in vivo* glycemia clearance 15 min after the arginine challenge (Q and R). Insulin secretion response to arginine was not significant (S). $n = 5–7$.
(T and U) Membrane potential recordings in β cells from (T) control or (U) *Hnf1a*^{iPanKO} islets. A solution containing 5 mM glucose and 10 mM arginine was added as indicated. $n = 4$ from 4 untreated control mice or $n = 4$ from 3 *Hnf1a*^{iPanKO} mice.
(V) Summary of recordings in (T) and (U), percentage of cells showing action potential firing (AP, blue) and no action potentials (no AP, orange) during application of 10 mM arginine in untreated control ($n = 4$) and *Hnf1a*^{iPanKO} ($n = 5$) β cells.
Student's t test was used on (B), (C), (E), (F), (H), (I), (K)–(N) (bar plots), (P), (R), and (S). $^{*}p < 0.05$, $^{**}p < 0.01$, $^{***}p < 0.001$, $^{****}p < 0.0001$. Graphs depict means ± SEM.
See also Figure S5.

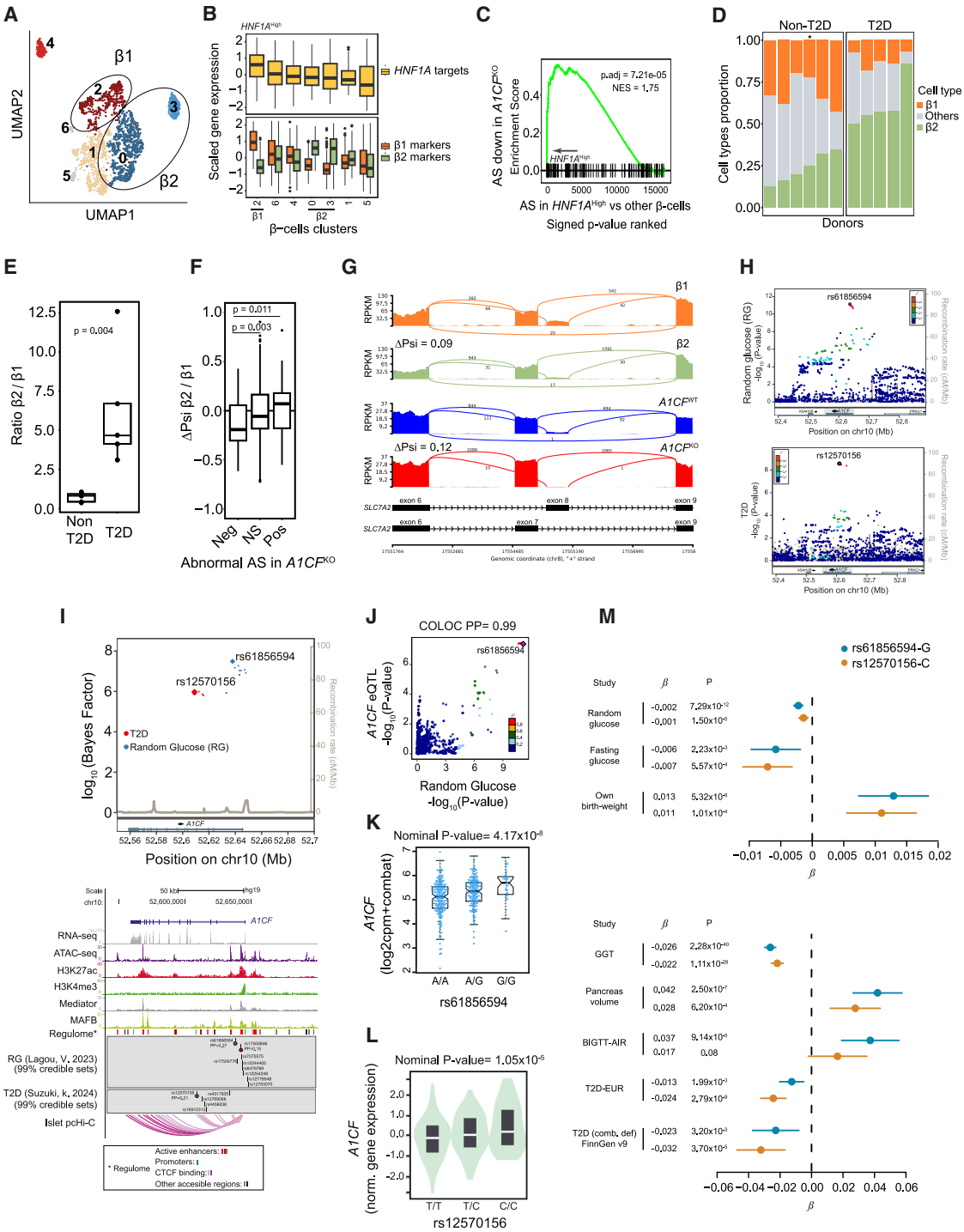

Figure 7. A1CF-dependent splicing in β cells and T2D

(A) UMAP representation of Seurat-defined Vasa-seq clusters of β cells. Based on previously identified gene signatures shown in (B), cluster 2 was annotated as β1 state, whereas clusters 0 and 3 as β2 state.

(B) Scaled expression for (top) 172 HNF1A target genes and (bottom) genes from previously defined β1 and β2 signatures for each cluster shown in (A). Cluster 2 is enriched in HNF1A targets and β1 genes, while clusters 0 and 3 show enriched expression of β2 genes.

(C) Gene set enrichment analysis (GSEA) shows that alternative splicing (AS) events with decreased exon inclusion in *A1CF*^{KO} (FDR < 0.05 and ΔPsi < −0.1) are enriched among events showing higher inclusion in *HNF1A*^{High} vs. other β cells, ranked by their signed *p* value.

(D) Proportion of β1, β2, and other β cells for each T2D or non-T2D donor. The star indicates a normoglycemic donor previously diagnosed with diabetes in remission.

(legend continued on next page)

transcription and splicing gene expression program. We provide functional and genetic evidence that implicates this pathway in human β cell physiology and diabetes.

In contrast to the wealth of knowledge concerning transcription mechanisms governing β cell identity and diabetes,[84,85] the role of RNA splicing remains very poorly explored. Recent studies have shown circadian regulation of splicing of islet transcripts involved in insulin release,[86] while other studies revealed a handful of splicing regulators in β cells, including ELAVL4, NOVA2, RBFOX2, SMNDC1, or the microexon splicing regulator SRRM3.[87–90] Interestingly, most of these factors appear to regulate splicing programs shared with neural cell types, in keeping with the notion that—despite their endodermal origin—β cells are electrically excitable neuroendocrine cells that share core neural gene expression programs.[91,92] The A1CF-dependent splicing β cell program, by contrast, targets a distinct set of epithelial functions, including genes regulating cilia, or intracellular protein trafficking through the ER and Golgi apparatus. This HNF1A-A1CF axis, therefore, appears to drive a non-neural component of the specialized β cell gene expression program.

The mechanisms that ensure the cell-type specificity of RNA splicing programs are poorly understood. There is extensive evidence for cell-type-specific post-transcriptional regulation of splicing regulators via splicing factor networks,[30,93] exemplified by the sex-specific regulation of *Drosophila* sex lethal.[94,95] How cell-type-specific transcription and splicing networks are coordinated is less clear. Acute gene inhibition or overexpression studies have shown that selected lineage-restricted transcription factors, such as REST[96], MYOD,[97] Glis3,[98] or Nacc1,[31] regulate splicing factor genes, although genetic models have not been used to address their *in vivo* impact on cell-specific expression of splicing factors and the downstream splicing programs. Our studies show that A1CF expression is remarkably restricted to HNF1A-expressing tissues, while A1CF dependence on HNF1A is conserved across mouse and human islet cells. The results suggest a model whereby HNF1A coordinates cell-type-specific expression through the direct regulation of transcription of hundreds of genes and indirectly through a splicing pathway that targets a largely separate set of genes. This provides an example of an RNA splicing program that is essentially an integral component of a cell-specific gene expression program controlled by an individual transcription factor.

HNF1A regulates numerous genes in β cells, and HNF1A-deficient β cell failure is likely caused by the combined effect of multiple molecular defects. While the exact contribution of RNA splicing abnormalities is difficult to define, several observations suggest that A1CF is one of the key components of the β cell HNF1A-dependent regulatory network. First, natural variants that increase *A1CF* expression in human islets exhibit expected associations with improved insulin secretion and glycemic traits or T2D risk. Second, *A1CF* deficiency, as well as *HNF1A* deficiency, caused abnormal splicing of numerous genes with established roles in β cell signaling and secretion.[37,55–61,99–101] Among these, *A1CF* and *HNF1A* mutants led to an isoform switch in the *SLC7A2* arginine transporter. This caused decreased expression of the low-affinity, high-capacity *SLC7A2* isoform that has been previously implicated in arginine-regulated insulin secretion[63,64] and, expectedly, led to defective arginine-induced insulin secretion. This observation raises an intriguing, but testable, possibility that dietary supplementation with arginine could be harnessed to overcome abnormal *SLC7A2* splicing for improving β cell function in HNF1A-deficient diabetes.

Taken together, the evidence from single-cell genomics, integrative genetics, and functional studies suggests that *A1CF*-dependent splicing abnormalities constitute a core defect in the molecular pathophysiology of HNF1A-deficient monogenic diabetes and T2D. This knowledge can open therapeutic avenues for HNF1A-deficient diabetes that leverage splicing modulation,[102] either through compounds that target splicing complexes or with β cell-directed oligonucleotides that force the inclusion or exclusion of selected exons, thereby ameliorating impaired β cell functionality. More generally, our findings exemplify how an upstream defect in a transcription-splicing regulatory axis can lead to RNA splicing abnormalities in the pathogenesis of diabetes mellitus.

Limitations of the study

This study reveals an evolutionarily conserved linear hierarchy that coordinates cell-specific transcription and splicing programs. Further work is needed to understand whether this is how other cell-specific transcription and splicing programs are coordinated. Alternative models include a more distributed dependence of cell-specific splicing factor genes on multiple

(E) β2/β1 cell ratio was ∼8-fold increased in T2D vs. non-T2D donors (Wilcoxon $p = 0.004$).
(F) ΔPsi values for β2 vs. β1 cells were filtered for nominal $p < 0.05$ and separated according to splicing events showing decreased, non-significant, or increased exon inclusion in *A1CF*^{KO} cells. AS events in *A1CF*^{KO} cells were defined as FDR < 0.05 and ΔPsi <−0.1 or >0.1. Wilcoxon *p* values are shown. Error bars depict 95% CI.
(G) *SLC7A2* exon 7 and 8 splicing for β1 and β2 subpopulations (top) and *A1CF*^{KO} or control cells (bottom).
(H) Random glucose (RG) and T2D genetic association *p* values in −log10 scale (*y* axis) and hg19 genomic locations (*x* axis). Variant colors depict LD correlation (r^2) with lead RG or T2D variants.
(I) 99% credible set of candidate causal variants for RG (blue) and T2D (red) associations. Diamonds depict lead RG and T2D variants. Below, in the same scale, human islet assay for transposase-accessible chromatin using sequencing (ATAC-seq) and ChIP-seq tracks, fine-mapped RG and T2D variants, and promoter capture Hi-C (pcHi-C) interactions in pink, showing proximity between the *A1CF* promoter and enhancers containing the lead T2D variant or a credible variant (red) that has $r^2 = 1$ with the lead RG variant (purple dot).
(J) COMBAT normalized *A1CF* expression in human islets for the RG lead variant.
(K) LocusCompare plot for islet *A1CF* eQTL and RG *p* values ($-\log_{10}$).
(L) Normalized *A1CF* expression in pancreas (GTEx) for the T2D lead variant.
(M) Forest plot of associations for lead RG (rs61856594) and T2D (rs12570156) variants, showing β estimates and 95% confidence intervals for the A1CF-increasing allele. GGT, gamma glutamyl transferase; BIGTT-AIR, β cell function, glucose tolerance, and acute insulin response.
See also Figure S6.

cell-specific transcription factors or scenarios in which the cellular specificity of splicing programs is predominantly regulated post-transcriptionally, as shown for numerous examples of cross-regulatory interactions between splicing factors.[93–95]

Our mouse genetic studies indicate that β cell-autonomous defects cause HNF1A-deficient diabetes. We cannot rule out contributions from other HNF1A-expressing lineages in any untested environmental or human-specific contexts. On the other hand, unchallenged *Hnf1a*^{pKO} and *Hnf1a*^{βKO} mice did not show conspicuous changes in β cell mass, indicating that diabetes in these models primarily results from β cell dysfunction. However, β cell proliferation changes have been documented in mutant mice and cell lines,[14] which can plausibly translate to impaired β cell mass as an additional contributing mechanism.

This study integrates experimental perturbations with human genetic studies to show that the A1CF-dependent branch of the HNF1A-dependent network is important for β cell function. However, it is crucial to acknowledge that both HNF1A and A1CF control broad gene programs. Therefore, our findings do not imply that the functional role of HNF1A in β cells is restricted to its regulation of *A1CF* transcription, nor that of A1CF to *SLC7A2* splicing.

RESOURCE AVAILABILITY

Lead contact

Further information and requests for resources and reagents should be directed to the lead contact, Jorge Ferrer (jorge.ferrer@crg.eu).

Materials availability

Reagents generated in this study are available from the lead contact with a completed material transfer agreement. The following constructs have been deposited in Addgene: LentiCMV-HNF1A, #204379; LentiCMV-A1CF, #204377; and LentiCMV-controlEGFP, #204387.

Data and code availability

- Data used to generate manuscript figures are provided in Tables S1, S2, S3, S4, S5, S6, S7, S8, and S9 and Data S1, which contains unprocessed raw data underlying the uncropped western blots, HNF1A binding data, and graphs related to Figures 1, 2, 3, 4, 5, 6, 7, S1, S2, S4, and S5.
- Raw sequencing reads from RNA-seq and ChIP-seq have been deposited in the GEO public repository under accession numbers GEO: GSE277551 and GEO: GSE277552, respectively.
- We reanalyzed human islet scRNA-seq and VASA-seq reads from the ESPACE Human Cell Atlas. Human islet ChIP-seq data were obtained from EGA: EGAS00001002917 and ArrayExpress: E-MTAB-1919.[69,71,103] We reanalyzed mouse liver RNA-seq from the NCBI Sequence Read Archive (SRA: PRJNA530736).[48] Processed data files, including binding sites from ChIP-seq data and pc-HiC interactions, are deposited at https://www.crg.eu/en/programmes-groups/ferrer-lab#datasets. Scripts developed for this study are available from the lead contact upon request.

ACKNOWLEDGMENTS

This research was supported by Ministerio de Ciencia e Innovación (PID2021-122522OB-I00), Medical Research Council (MR/L02036X/1), a European Research Council Advanced Grant (789055), Departament de Recerca i Universitats de la Generalitat de Catalunya (SGR2021-01371), and ESPACE Human Cell Atlas consortium (EUHorizon2020 874710). Work in CRG was supported by the CERCA Programme, Generalitat de Catalunya, Centro de Excelencia Severo Ochoa (CEX2020-001049), and the Spanish Ministry of Science and Innovation to the EMBL partnership. D.B. was supported by EMBO Long-Term Fellowship ALT295-2019, the 2022 EFSD Rising Star Programme, and the Ministerio de Ciencia e Innovación Ramón y Cajal program RYC2021-033131-I. M.C.-A. was supported by the Boehringer Ingelheim Fonds PhD fellowship. F.M. is funded by a Marie Skłodowska-Curie postdoctoral fellowship. We thank CRG Flow Cytometry, Tissue Engineering, and Genomics Units; NIHR Imperial BRC Genomics; Klaus Kaestner (University of Pennsylvania); and Chris Wright and Maureen Gannon (Vanderbilt University) for mouse lines. Studies at the University of Gothenburg were supported by an International Recruitment Award from the Swedish Research Council (2013-7107 to P. Rorsman). We thank Corali Cros and Aina Bernal for lab support and stem cell culture, Carmen Sanahuja for management, and Manuel Irimia and Juan Valcarcel for helpful discussions.

AUTHOR CONTRIBUTIONS

M.G.D.V., E.B., and J.F. conceptualized and designed the study. E.B., M.G.D.V., D.B., M.C.-A., S.B.-G., F.M., M.P.-F., and J.F. contributed to experimental design, interpreted results, and wrote the manuscript. M.G.D.V., E.B., M.A.M., D.B., and M.C.-A. generated and interpreted experimental data; J.G.-H. and M.A.M. designed or characterized animal models; S.M. performed cell culture and generation of immortalized and stem cell lines; H.D. and P. Rorsman performed electrophysiological studies; S.B.-G. performed human genetic analysis; and F.M., M.P.-F., and M.T.-D. performed single-cell analysis, using data generated by J.G.-H., N.G., H.H., A.v.O., E.d.K., C.C., and R.E. All authors provided input to data interpretation and revision of the manuscript.

DECLARATION OF INTERESTS

P. Ravassard is a shareholder at Human Cell Design (HCD).

STAR★METHODS

Detailed methods are provided in the online version of this paper and include the following:

- KEY RESOURCES TABLE
- EXPERIMENTAL MODEL AND SUBJECT DETAILS
  - Animal studies
  - Human embryonic kidney 293 FT (HEK293FT)
  - MIN6
  - Generation of EndoC-βH3 mutant models
  - Generation and differentiation of stem cell models
- METHOD DETAILS
  - General cell culture methods
  - Mouse pancreatic islet isolation
  - Glucose homeostasis studies
  - Immunofluorescence staining
  - β-cell area quantification
  - Lentivirus production and transduction of EndoC-βH3 and SC-islets
  - SSO and ASO experiments
  - In vitro insulin secretion studies
  - Electrophysiological recordings of mouse islets
  - RNA extraction
  - Quantitative PCR (qPCR)
  - RNA-seq and differential gene expression
  - Western blotting
  - Functional enrichment analysis
  - Differential alternative splicing
  - ChIP-seq
  - Motif analysis
  - Data visualization
  - VASA-seq single-cell transcriptome and differential splicing analysis
  - Co-expression analysis
- QUANTIFICATION AND STATISTICAL ANALYSIS
  - Visualization of genetic associations
  - Genetic fine-mapping
  - Colocalization analysis
  - Transcriptome-Wide Association Studies

SUPPLEMENTAL INFORMATION

Supplemental information can be found online at https://doi.org/10.1016/j.cmet.2025.07.007.

Received: August 22, 2024
Revised: February 27, 2025
Accepted: July 9, 2025
Published: August 6, 2025

REFERENCES

1. Yamagata, K., Oda, N., Kaisaki, P.J., Menzel, S., Furuta, H., Vaxillaire, M., Southam, L., Cox, R.D., Lathrop, G.M., Boriraj, V.V., et al. (1996). Mutations in the hepatocyte nuclear factor-1alpha gene in maturity-onset diabetes of the young (MODY3). Nature *384*, 455–458. https://doi.org/10.1038/384455a0.
2. Estrada, K., Aukrust, I., Bjørkhaug, L., Burtt, N.P., Mercader, J.M., García-Ortiz, H., Huerta-Chagoya, A., Moreno-Macías, H., Walford, G., et al.; SIGMA; Type 2 Diabetes Consortium (2014). Association of a low-frequency variant in HNF1A with type 2 diabetes in a Latino population. JAMA *311*, 2305–2314. https://doi.org/10.1001/jama.2014.6511.
3. Kwak, S.H., Srinivasan, S., Chen, L., Todd, J., Mercader, J., Jensen, E., Divers, J., Mottl, A., Pihoker, C., Gandica, R., et al. (2023). Insights from rare variants into the genetic architecture and biology of youth-onset type 2 diabetes. https://doi.org/10.21203/rs.3.rs-2886343/v1.
4. Mahajan, A., Wessel, J., Willems, S.M., Zhao, W., Robertson, N.R., Chu, A.Y., Gan, W., Kitajima, H., Taliun, D., Rayner, N.W., et al. (2018). Refining the accuracy of validated target identification through coding variant fine-mapping in type 2 diabetes. Nat. Genet. *50*, 559–571. https://doi.org/10.1038/s41588-018-0084-1.
5. Thuesen, A.C.B., Stæger, F.F., Kaci, A., Solheim, M.H., Aukrust, I., Jørsboe, E., Santander, C.G., Andersen, M.K., Li, Z., Gilly, A., et al. (2023). A novel splice-affecting HNF1A variant with large population impact on diabetes in Greenland. Lancet Reg Health Eur. *24*, 100529. https://doi.org/10.1016/j.lanepe.2022.100529.
6. Najmi, L.A., Aukrust, I., Flannick, J., Molnes, J., Burtt, N., Molven, A., Groop, L., Altshuler, D., Johansson, S., Bjørkhaug, L., et al. (2017). Functional investigations of HNF1A identify rare variants as risk factors for type 2 diabetes in the general population. Diabetes *66*, 335–346. https://doi.org/10.2337/db16-0460.
7. DeForest, N., Kavitha, B., Hu, S., Isaac, R., Krohn, L., Wang, M., Du, X., De Arruda Saldanha, C., Gylys, J., Merli, E., et al. (2023). Human gain-of-function variants in HNF1A confer protection from diabetes but independently increase hepatic secretion of atherogenic lipoproteins. Cell Genom. *3*, 100339. https://doi.org/10.1016/j.xgen.2023.100339.
8. Weng, C., Gu, A., Zhang, S., Lu, L., Ke, L., Gao, P., Liu, X., Wang, Y., Hu, P., Plummer, D., et al. (2023). Single cell multiomic analysis reveals diabetes-associated β-cell heterogeneity driven by HNF1A. Nat. Commun. *14*, 5400. https://doi.org/10.1038/s41467-023-41228-3.
9. Wang, G., Chiou, J., Zeng, C., Miller, M., Matta, I., Han, J.Y., Kadakia, N., Okino, M.L., Beebe, E., Mallick, M., et al. (2023). Integrating genetics with single-cell multiomic measurements across disease states identifies mechanisms of beta cell dysfunction in type 2 diabetes. Nat. Genet. *55*, 984–994. https://doi.org/10.1038/s41588-023-01397-9.
10. Lee, Y.H., Sauer, B., and Gonzalez, F.J. (1998). Laron dwarfism and non-insulin-dependent diabetes mellitus in the Hnf-1alpha knockout mouse. Mol. Cell. Biol. *18*, 3059–3068. https://doi.org/10.1128/MCB.18.5.3059.
11. Pontoglio, M., Sreenan, S., Roe, M., Pugh, W., Ostrega, D., Doyen, A., Pick, A.J., Baldwin, A., Velho, G., Froguel, P., et al. (1998). Defective insulin secretion in hepatocyte nuclear factor 1alpha-deficient mice. J. Clin. Invest. *101*, 2215–2222. https://doi.org/10.1172/JCI2548.
12. Haliyur, R., Tong, X., Sanyoura, M., Shrestha, S., Lindner, J., Saunders, D.C., Aramandla, R., Poffenberger, G., Redick, S.D., Bottino, R., et al. (2019). Human islets expressing HNF1A variant have defective β cell transcriptional regulatory networks. J. Clin. Invest. *129*, 246–251. https://doi.org/10.1172/JCI121994.
13. Byrne, M.M., Sturis, J., Menzel, S., Yamagata, K., Fajans, S.S., Dronsfield, M.J., Bain, S.C., Hattersley, A.T., Velho, G., Froguel, P., et al. (1996). Altered insulin secretory responses to glucose in diabetic and nondiabetic subjects with mutations in the diabetes susceptibility gene MODY3 on chromosome 12. Diabetes *45*, 1503–1510. https://doi.org/10.2337/diab.45.11.1503.
14. Servitja, J.M., Pignatelli, M., Maestro, M.A., Cardalda, C., Boj, S.F., Lozano, J., Blanco, E., Lafuente, A., McCarthy, M.I., Sumoy, L., et al. (2009). Hnf1alpha (MODY3) controls tissue-specific transcriptional programs and exerts opposed effects on cell growth in pancreatic islets and liver. Mol. Cell. Biol. *29*, 2945–2959. https://doi.org/10.1128/MCB.01389-08.
15. Shih, D.Q., Bussen, M., Sehayek, E., Ananthanarayanan, M., Shneider, B.L., Suchy, F.J., Shefer, S., Bollileni, J.S., Gonzalez, F.J., Breslow, J.L., et al. (2001). Hepatocyte nuclear factor-1alpha is an essential regulator of bile acid and plasma cholesterol metabolism. Nat. Genet. *27*, 375–382. https://doi.org/10.1038/86871.
16. Kalisz, M., Bernardo, E., Beucher, A., Maestro, M.A., Del Pozo, N., Millán, I., Haeberle, L., Schlensog, M., Safi, S.A., Knoefel, W.T., et al. (2020). HNF1A recruits KDM6A to activate differentiated acinar cell programs that suppress pancreatic cancer. EMBO J. *39*, e102808. https://doi.org/10.15252/embj.2019102808.
17. D'Angelo, A., Bluteau, O., Garcia-Gonzalez, M.A., Gresh, L., Doyen, A., Garbay, S., Robine, S., and Pontoglio, M. (2010). Hepatocyte nuclear factor 1alpha and beta control terminal differentiation and cell fate commitment in the gut epithelium. Development *137*, 1573–1582. https://doi.org/10.1242/dev.044420.
18. Boj, S.F., Parrizas, M., Maestro, M.A., and Ferrer, J. (2001). A transcription factor regulatory circuit in differentiated pancreatic cells. Proc. Natl. Acad. Sci. USA *98*, 14481–14486. https://doi.org/10.1073/pnas.241349398.
19. Baraille, F., Ayari, S., Carrière, V., Osinski, C., Garbin, K., Blondeau, B., Guillemain, G., Serradas, P., Rousset, M., Lacasa, M., et al. (2015). Glucose tolerance is improved in mice invalidated for the nuclear receptor HNF-4γ: a critical role for enteroendocrine cell lineage. Diabetes *64*, 2744–2756. https://doi.org/10.2337/db14-0993.
20. De Vadder, F., Kovatcheva-Datchary, P., Goncalves, D., Vinera, J., Zitoun, C., Duchampt, A., Bäckhed, F., and Mithieux, G. (2014). Microbiota-generated metabolites promote metabolic benefits via gut-brain neural circuits. Cell *156*, 84–96. https://doi.org/10.1016/j.cell.2013.12.016.
21. Gribble, F.M., and Reimann, F. (2019). Function and mechanisms of enteroendocrine cells and gut hormones in metabolism. Nat. Rev. Endocrinol. *15*, 226–237. https://doi.org/10.1038/s41574-019-0168-8.
22. El Ouaamari, A., Kawamori, D., Dirice, E., Liew, C.W., Shadrach, J.L., Hu, J., Katsuta, H., Hollister-Lock, J., Qian, W.J., Wagers, A.J., et al. (2013). Liver-derived systemic factors drive beta cell hyperplasia in insulin-resistant states. Cell Rep. *3*, 401–410. https://doi.org/10.1016/j.celrep.2013.01.007.
23. El Ouaamari, A., Dirice, E., Gedeon, N., Hu, J., Zhou, J.Y., Shirakawa, J., Hou, L., Goodman, J., Karampelias, C., Qiang, G., et al. (2016). SerpinB1 promotes pancreatic β cell proliferation. Cell Metab. *23*, 194–205. https://doi.org/10.1016/j.cmet.2015.12.001.
24. Cui, X., Feng, J., Wei, T., Zhang, L., Lang, S., Yang, K., Yang, J., Liu, J., Sterr, M., Lickert, H., et al. (2023). Pancreatic alpha cell glucagon-liver FGF21 axis regulates beta cell regeneration in a mouse model of type 2 diabetes. Diabetologia *66*, 535–550. https://doi.org/10.1007/s00125-022-05822-2.
25. Low, B.S.J., Lim, C.S., Ding, S.S.L., Tan, Y.S., Ng, N.H.J., Krishnan, V.G., Ang, S.F., Neo, C.W.Y., Verma, C.S., Hoon, S., et al. (2021). Decreased GLUT2 and glucose uptake contribute to insulin secretion defects in MODY3/HNF1A hiPSC-derived mutant β cells. Nat. Commun. *12*, 3133. https://doi.org/10.1038/s41467-021-22843-4.

26. Dukes, I.D., Sreenan, S., Roe, M.W., Levisetti, M., Zhou, Y.P., Ostrega, D., Bell, G.I., Pontoglio, M., Yaniv, M., Philipson, L., et al. (1998). Defective pancreatic beta-cell glycolytic signaling in hepatocyte nuclear factor-1alpha-deficient mice. J. Biol. Chem. *273*, 24457–24464. https://doi.org/10.1074/jbc.273.38.24457.

27. Cardenas-Diaz, F.L., Osorio-Quintero, C., Diaz-Miranda, M.A., Kishore, S., Leavens, K., Jobaliya, C., Stanescu, D., Ortiz-Gonzalez, X., Yoon, C., Chen, C.S., et al. (2019). Modeling monogenic diabetes using human ESCs reveals developmental and metabolic deficiencies caused by mutations in HNF1A. Cell Stem Cell *25*, 273–289.e5. https://doi.org/10.1016/j.stem.2019.07.007.

28. González, B.J., Zhao, H., Niu, J., Williams, D.J., Lee, J., Goulbourne, C. N., Xing, Y., Wang, Y., Oberholzer, J., Blumenkrantz, M.H., et al. (2022). Reduced calcium levels and accumulation of abnormal insulin granules in stem cell models of HNF1A deficiency. Commun. Biol. *5*, 779. https://doi.org/10.1038/s42003-022-03696-z.

29. Hermann, F.M., Kjærgaard, M.F., Tian, C., Tiemann, U., Jackson, A., Olsen, L.R., Kraft, M., Carlsson, P.O., Elfving, I.M., Kettunen, J.L.T., et al. (2023). An insulin hypersecretion phenotype precedes pancreatic β cell failure in MODY3 patient-specific cells. Cell Stem Cell *30*, 38–51. e8. https://doi.org/10.1016/j.stem.2022.12.001.

30. Jangi, M., and Sharp, P.A. (2014). Building robust transcriptomes with master splicing factors. Cell *159*, 487–498. https://doi.org/10.1016/j.cell.2014.09.054.

31. Han, H., Braunschweig, U., Gonatopoulos-Pournatzis, T., Weatheritt, R. J., Hirsch, C.L., Ha, K.C.H., Radovani, E., Nabeel-Shah, S., Sterne-Weiler, T., Wang, J., et al. (2017). Multilayered control of alternative splicing regulatory networks by transcription factors. Mol. Cell *65*, 539–553.e7. https://doi.org/10.1016/j.molcel.2017.01.011.

32. Parviz, F., Li, J., Kaestner, K.H., and Duncan, S.A. (2002). Generation of a conditionally null allele of hnf4alpha. Genesis *32*, 130–133. https://doi.org/10.1002/gene.10058.

33. Tan, J., Xu, J., Wei, G., Zhang, L., Sun, L., Wang, G., Li, F., and Jiang, F. (2019). HNF1α controls liver lipid metabolism and insulin resistance via negatively regulating the SOCS-3-STAT3 signaling pathway. J. Diabetes Res. *2019*, 5483946. https://doi.org/10.1155/2019/5483946.

34. Madison, B.B., Dunbar, L., Qiao, X.T., Braunstein, K., Braunstein, E., and Gumucio, D.L. (2002). Cis elements of the villin gene control expression in restricted domains of the vertical (crypt) and horizontal (duodenum, cecum) axes of the intestine. J. Biol. Chem. *277*, 33275–33283. https://doi.org/10.1074/jbc.M204935200.

35. Hingorani, S.R., Petricoin, E.F., Maitra, A., Rajapakse, V., King, C., Jacobetz, M.A., Ross, S., Conrads, T.P., Veenstra, T.D., Hitt, B.A., et al. (2003). Preinvasive and invasive ductal pancreatic cancer and its early detection in the mouse. Cancer Cell *4*, 437–450. https://doi.org/10.1016/s1535-6108(03)00309-x.

36. Campbell, J.E., and Drucker, D.J. (2015). Islet α cells and glucagon–critical regulators of energy homeostasis. Nat. Rev. Endocrinol. *11*, 329–338. https://doi.org/10.1038/nrendo.2015.51.

37. Rorsman, P., and Ashcroft, F.M. (2018). Pancreatic β-cell electrical activity and insulin secretion: of mice and men. Physiol. Rev. *98*, 117–214. https://doi.org/10.1152/physrev.00008.2017.

38. Østoft, S.H., Bagger, J.I., Hansen, T., Hartmann, B., Pedersen, O., Holst, J.J., Knop, F.K., and Vilsbøll, T. (2015). Postprandial incretin and islet hormone responses and dipeptidyl-peptidase 4 enzymatic activity in patients with maturity onset diabetes of the young. Eur. J. Endocrinol. *173*, 205–215. https://doi.org/10.1530/EJE-15-0070.

39. Østoft, S.H., Bagger, J.I., Hansen, T., Pedersen, O., Holst, J.J., Knop, F. K., and Vilsbøll, T. (2014). Incretin effect and glucagon responses to oral and intravenous glucose in patients with maturity-onset diabetes of the young–type 2 and type 3. Diabetes *63*, 2838–2844. https://doi.org/10.2337/db13-1878.

40. Ackermann, A.M., Zhang, J., Heller, A., Briker, A., and Kaestner, K.H. (2017). High-fidelity Glucagon-CreER mouse line generated by CRISPR-Cas9 assisted gene targeting. Mol. Metab. *6*, 236–244. https://doi.org/10.1016/j.molmet.2017.01.003.

41. Thorens, B., Tarussio, D., Maestro, M.A., Rovira, M., Heikkilä, E., and Ferrer, J. (2015). Ins1(Cre) knock-in mice for beta cell-specific gene recombination. Diabetologia *58*, 558–565. https://doi.org/10.1007/s00125-014-3468-5.

42. Benazra, M., Lecomte, M.J., Colace, C., Müller, A., Machado, C., Pechberty, S., Bricout-Neveu, E., Grenier-Godard, M., Solimena, M., Scharfmann, R., et al. (2015). A human beta cell line with drug inducible excision of immortalizing transgenes. Mol. Metab. *4*, 916–925. https://doi.org/10.1016/j.molmet.2015.09.008.

43. Boj, S.F., Petrov, D., and Ferrer, J. (2010). Epistasis of transcriptomes reveals synergism between transcriptional activators Hnf1alpha and Hnf4alpha. PLoS Genet. *6*, e1000970. https://doi.org/10.1371/journal.pgen.1000970.

44. Shih, D.Q., Screenan, S., Munoz, K.N., Philipson, L., Pontoglio, M., Yaniv, M., Polonsky, K.S., and Stoffel, M. (2001). Loss of HNF-1alpha function in mice leads to abnormal expression of genes involved in pancreatic islet development and metabolism. Diabetes *50*, 2472–2480. https://doi.org/10.2337/diabetes.50.11.2472.

45. Beucher, A., Miguel-Escalada, I., Balboa, D., De Vas, M.G., Maestro, M. A., Garcia-Hurtado, J., Bernal, A., Gonzalez-Franco, R., Vargiu, P., Heyn, H., et al. (2022). The HASTER lncRNA promoter is a cis-acting transcriptional stabilizer of HNF1A. Nat. Cell Biol. *24*, 1528–1540. https://doi.org/10.1038/s41556-022-00996-8.

46. Fossat, N., Tourle, K., Radziewic, T., Barratt, K., Liebhold, D., Studdert, J. B., Power, M., Jones, V., Loebel, D.A.F., and Tam, P.P.L. (2014). C to U RNA editing mediated by APOBEC1 requires RNA-binding protein RBM47. EMBO Rep. *15*, 903–910. https://doi.org/10.15252/embr.201438450.

47. Snyder, E.M., McCarty, C., Mehalow, A., Svenson, K.L., Murray, S.A., Korstanje, R., and Braun, R.E. (2017). APOBEC1 complementation factor (A1CF) is dispensable for C-to-U RNA editing in vivo. Rna *23*, 457–465. https://doi.org/10.1261/rna.058818.116.

48. Nikolaou, K.C., Vatandaslar, H., Meyer, C., Schmid, M.W., Tuschl, T., and Stoffel, M. (2019). The RNA-binding protein A1CF regulates hepatic fructose and glycerol metabolism via alternative RNA splicing. Cell Rep. *29*, 283–300.e8. https://doi.org/10.1016/j.celrep.2019.08.100.

49. Cieply, B., Park, J.W., Nakauka-Ddamba, A., Bebee, T.W., Guo, Y., Shang, X., Lengner, C.J., Xing, Y., and Carstens, R.P. (2016). Multiphasic and dynamic changes in alternative splicing during induction of pluripotency are coordinated by numerous RNA-binding proteins. Cell Rep. *15*, 247–255. https://doi.org/10.1016/j.celrep.2016.03.025.

50. Shen, S., Park, J.W., Lu, Z.X., Lin, L., Henry, M.D., Wu, Y.N., Zhou, Q., and Xing, Y. (2014). rMATS: robust and flexible detection of differential alternative splicing from replicate RNA-seq data. Proc. Natl. Acad. Sci. USA *111*, E5593–E5601. https://doi.org/10.1073/pnas.1419161111.

51. Fang, J., Liu, M., Zhang, X., Sakamoto, T., Taatjes, D.J., Jena, B.P., Sun, F., Woods, J., Bryson, T., Kowluru, A., et al. (2015). COPII-dependent ER export: a critical component of insulin biogenesis and beta-cell ER homeostasis. Mol. Endocrinol. *29*, 1156–1169. https://doi.org/10.1210/me.2015-1012.

52. Bond, L.M., Peden, A.A., Kendrick-Jones, J., Sellers, J.R., and Buss, F. (2011). Myosin VI and its binding partner optineurin are involved in secretory vesicle fusion at the plasma membrane. Mol. Biol. Cell *22*, 54–65. https://doi.org/10.1091/mbc.E10-06-0553.

53. Gerdes, H.H. (2008). Membrane traffic in the secretory pathway. Cell. Mol. Life Sci. *65*, 2779–2780. https://doi.org/10.1007/s00018-008-8348-z.

54. Jha, A., K Aicher, J., R Gazzara, M., Singh, D., and Barash, Y. (2020). Enhanced integrated gradients: improving interpretability of deep learning models using splicing codes as a case study. Genome Biol. *21*, 149. https://doi.org/10.1186/s13059-020-02055-7.

55. Chang, G., Yang, R., Cao, Y., Nie, A., Gu, X., and Zhang, H. (2016). SIDT2 is involved in the NAADP-mediated release of calcium from insulin

secretory granules. J. Mol. Endocrinol. *56*, 249–259. https://doi.org/10.1530/JME-15-0227.

56. Xiong, X., Wang, G., Tao, R., Wu, P., Kono, T., Li, K., Ding, W.X., Tong, X., Tersey, S.A., Harris, R.A., et al. (2016). Sirtuin 6 regulates glucose-stimulated insulin secretion in mouse pancreatic beta cells. Diabetologia *59*, 151–160. https://doi.org/10.1007/s00125-015-3778-2.
57. Ohara-Imaizumi, M., Ohtsuka, T., Matsushima, S., Akimoto, Y., Nishiwaki, C., Nakamichi, Y., Kikuta, T., Nagai, S., Kawakami, H., Watanabe, T., et al. (2005). ELKS, a protein structurally related to the active zone-associated protein CAST, is expressed in pancreatic beta cells and functions in insulin exocytosis: interaction of ELKS with exocytotic machinery analyzed by total internal reflection fluorescence microscopy. Mol. Biol. Cell *16*, 3289–3300. https://doi.org/10.1091/mbc.e04-09-0816.
58. Jansson, D., Ng, A.C.H., Fu, A., Depatie, C., Al Azzabi, M., and Screaton, R.A. (2008). Glucose controls CREB activity in islet cells via regulated phosphorylation of TORC2. Proc. Natl. Acad. Sci. USA *105*, 10161–10166. https://doi.org/10.1073/pnas.0800796105.
59. Lee, E.K., Kim, W., Tominaga, K., Martindale, J.L., Yang, X., Subaran, S. S., Carlson, O.D., Mercken, E.M., Kulkarni, R.N., Akamatsu, W., et al. (2012). RNA-binding protein HuD controls insulin translation. Mol. Cell *45*, 826–835. https://doi.org/10.1016/j.molcel.2012.01.016.
60. Ansari, I.H., Longacre, M.J., Stoker, S.W., Kendrick, M.A., O'Neill, L.M., Zitur, L.J., Fernandez, L.A., Ntambi, J.M., and MacDonald, M.J. (2017). Characterization of Acyl-CoA synthetase isoforms in pancreatic beta cells: Gene silencing shows participation of ACSL3 and ACSL4 in insulin secretion. Arch. Biochem. Biophys. *618*, 32–43. https://doi.org/10.1016/j.abb.2017.02.001.
61. Kepner, E.M., Yoder, S.M., Oh, E., Kalwat, M.A., Wang, Z., Quilliam, L.A., and Thurmond, D.C. (2011). Cool-1/βPIX functions as a guanine nucleotide exchange factor in the cycling of Cdc42 to regulate insulin secretion. Am. J. Physiol. Endocrinol. Metab. *301*, E1072–E1080. https://doi.org/10.1152/ajpendo.00312.2011.
62. Ward, W.K., Bolgiano, D.C., McKnight, B., Halter, J.B., and Porte, D., Jr. (1984). Diminished B cell secretory capacity in patients with noninsulin-dependent diabetes mellitus. J. Clin. Invest. *74*, 1318–1328. https://doi.org/10.1172/JCI111542.
63. Smith, P.A., Sakura, H., Coles, B., Gummerson, N., Proks, P., and Ashcroft, F.M. (1997). Electrogenic arginine transport mediates stimulus-secretion coupling in mouse pancreatic beta-cells. J. Physiol. *499*, 625–635. https://doi.org/10.1113/jphysiol.1997.sp021955.
64. Closs, E.I., Boissel, J.P., Habermeier, A., and Rotmann, A. (2006). Structure and function of cationic amino acid transporters (CATs). J. Membr. Biol. *213*, 67–77. https://doi.org/10.1007/s00232-006-0875-7.
65. Kavanaugh, M.P., Wang, H., Zhang, Z., Zhang, W., Wu, Y.N., Dechant, E., North, R.A., and Kabat, D. (1994). Control of cationic amino acid transport and retroviral receptor functions in a membrane protein family. J. Biol. Chem. *269*, 15445–15450. https://doi.org/10.1016/S0021-9258(17)40699-5.
66. Salmen, F., De Jonghe, J., Kaminski, T.S., Alemany, A., Parada, G.E., Verity-Legg, J., Yanagida, A., Kohler, T.N., Battich, N., van den Brekel, F., et al. (2022). High-throughput total RNA sequencing in single cells using VASA-seq. Nat. Biotechnol. *40*, 1780–1793. https://doi.org/10.1038/s41587-022-01361-8.
67. Suzuki, K., Hatzikotoulas, K., Southam, L., Taylor, H.J., Yin, X., Lorenz, K. M., Mandla, R., Huerta-Chagoya, A., Melloni, G.E.M., Kanoni, S., et al. (2024). Genetic drivers of heterogeneity in type 2 diabetes pathophysiology. Nature *627*, 347–357. https://doi.org/10.1038/s41586-024-07019-6.
68. Lagou, V., Jiang, L., Ulrich, A., Zudina, L., González, K.S.G., Balkhiyarova, Z., Faggian, A., Maina, J.G., Chen, S., Todorov, P.V., et al. (2023). GWAS of random glucose in 476,326 individuals provide insights into diabetes pathophysiology, complications and treatment stratification. Nat. Genet. *55*, 1448–1461. https://doi.org/10.1038/s41588-023-01462-3.
69. Miguel-Escalada, I., Bonàs-Guarch, S., Cebola, I., Ponsa-Cobas, J., Mendieta-Esteban, J., Atla, G., Javierre, B.M., Rolando, D.M.Y., Farabella, I., Morgan, C.C., et al. (2019). Human pancreatic islet three-dimensional chromatin architecture provides insights into the genetics of type 2 diabetes. Nat. Genet. *51*, 1137–1148. https://doi.org/10.1038/s41588-019-0457-0.
70. Gusev, A., Ko, A., Shi, H., Bhatia, G., Chung, W., Penninx, B.W.J.H., Jansen, R., de Geus, E.J.C., Boomsma, D.I., Wright, F.A., et al. (2016). Integrative approaches for large-scale transcriptome-wide association studies. Nat. Genet. *48*, 245–252. https://doi.org/10.1038/ng.3506.
71. Atla, G., Bonàs-Guarch, S., Cuenca-Ardura, M., Beucher, A., Crouch, D. J.M., Garcia-Hurtado, J., Moran, I., Irimia, M., Prasad, R.B., et al.; T2DSystems Consortium (2022). Genetic regulation of RNA splicing in human pancreatic islets. Genome Biol. *23*, 196. https://doi.org/10.1186/s13059-022-02757-0.
72. Alonso, L., Piron, A., Morán, I., Guindo-Martínez, M., Bonàs-Guarch, S., Atla, G., Miguel-Escalada, I., Royo, R., Puiggròs, M., Garcia-Hurtado, X., et al. (2021). TIGER: The gene expression regulatory variation landscape of human pancreatic islets. Cell Rep. *37*, 109807. https://doi.org/10.1016/j.celrep.2021.109807.
73. Viñuela, A., Varshney, A., van de Bunt, M., Prasad, R.B., Asplund, O., Bennett, A., Boehnke, M., Brown, A.A., Erdos, M.R., Fadista, J., et al. (2020). Genetic variant effects on gene expression in human pancreatic islets and their implications for T2D. Nat. Commun. *11*, 4912. https://doi.org/10.1038/s41467-020-18581-8.
74. GTEx Consortium (2013). The Genotype-Tissue Expression (GTEx) project. Nat. Genet. *45*, 580–585. https://doi.org/10.1038/ng.2653.
75. Madsen, A.L., Bonàs-Guarch, S., Gheibi, S., Prasad, R., Vangipurapu, J., Ahuja, V., Cataldo, L.R., Dwivedi, O., Hatem, G., Atla, G., et al. (2024). Genetic architecture of oral glucose-stimulated insulin release provides biological insights into type 2 diabetes aetiology. Nat. Metab. *6*, 1897–1912. https://doi.org/10.1038/s42255-024-01140-6.
76. Warrington, N.M., Beaumont, R.N., Horikoshi, M., Day, F.R., Helgeland, Ø., Laurin, C., Bacelis, J., Peng, S., Hao, K., Feenstra, B., et al. (2019). Maternal and fetal genetic effects on birth weight and their relevance to cardio-metabolic risk factors. Nat. Genet. *51*, 804–814. https://doi.org/10.1038/s41588-019-0403-1.
77. Liu, Y., Basty, N., Whitcher, B., Bell, J.D., Sorokin, E.P., van Bruggen, N., Thomas, E.L., and Cule, M. (2021). Genetic architecture of 11 organ traits derived from abdominal MRI using deep learning. eLife *10*, e65554. https://doi.org/10.7554/eLife.65554.
78. Garin, I., Edghill, E.L., Akerman, I., Rubio-Cabezas, O., Rica, I., Locke, J. M., Maestro, M.A., Alshaikh, A., Bundak, R., del Castillo, G., et al. (2010). Recessive mutations in the INS gene result in neonatal diabetes through reduced insulin biosynthesis. Proc. Natl. Acad. Sci. USA *107*, 3105–3110. https://doi.org/10.1073/pnas.0910533107.
79. Hattersley, A.T., Beards, F., Ballantyne, E., Appleton, M., Harvey, R., and Ellard, S. (1998). Mutations in the glucokinase gene of the fetus result in reduced birth weight. Nat. Genet. *19*, 268–270. https://doi.org/10.1038/953.
80. Beaumont, R.N., Flatley, C., Vaudel, M., Wu, X., Chen, J., Moen, G.H., Skotte, L., Helgeland, Ø., Solé-Navais, P., Banasik, K., et al. (2023). Genome-wide association study of placental weight identifies distinct and shared genetic influences between placental and fetal growth. Nat. Genet. *55*, 1807–1819. https://doi.org/10.1038/s41588-023-01520-w.
81. Wright, J.J., Williams, J.M., Letourneau-Freiberg, L.R., Kandasamy, B., Reyes, D., Kanegusuku, A.G., Philipson, L., Greeley, S.A.W., Hilmes, M.A., Powers, A.C., et al. (2023). Insulin deficiency from insulin gene mutation leads to smaller pancreas. Diabetes Care *46*, 773–776. https://doi.org/10.2337/dc22-2082.
82. Jurgens, S.J., Pirruccello, J.P., Choi, S.H., Morrill, V.N., Chaffin, M., Lubitz, S.A., Lunetta, K.L., and Ellinor, P.T. (2023). Adjusting for common variant polygenic scores improves yield in rare variant association analyses. Nat. Genet. *55*, 544–548. https://doi.org/10.1038/s41588-023-01342-w.

83. Liu, D.J., Peloso, G.M., Yu, H., Butterworth, A.S., Wang, X., Mahajan, A., Saleheen, D., Emdin, C., Alam, D., Alves, A.C., et al. (2017). Exome-wide association study of plasma lipids in >300,000 individuals. Nat. Genet. *49*, 1758–1766. https://doi.org/10.1038/ng.3977.

84. Servitja, J.M., and Ferrer, J. (2004). Transcriptional networks controlling pancreatic development and beta cell function. Diabetologia *47*, 597–613. https://doi.org/10.1007/s00125-004-1368-9.

85. Wortham, M., and Sander, M. (2021). Transcriptional mechanisms of pancreatic β-cell maturation and functional adaptation. Trends Endocrinol. Metab. *32*, 474–487. https://doi.org/10.1016/j.tem.2021.04.011.

86. Marcheva, B., Perelis, M., Weidemann, B.J., Taguchi, A., Lin, H., Omura, C., Kobayashi, Y., Newman, M.V., Wyatt, E.J., McNally, E.M., et al. (2020). A role for alternative splicing in circadian control of exocytosis and glucose homeostasis. Genes Dev. *34*, 1089–1105. https://doi.org/10.1101/gad.338178.120.

87. Moss, N.D., Wells, K.L., Theis, A., Kim, Y.K., Spigelman, A.F., Liu, X., MacDonald, P.E., and Sussel, L. (2023). Modulation of insulin secretion by RBFOX2-mediated alternative splicing. Nat. Commun. *14*, 7732. https://doi.org/10.1038/s41467-023-43605-4.

88. Juan-Mateu, J., Rech, T.H., Villate, O., Lizarraga-Mollinedo, E., Wendt, A., Turatsinze, J.V., Brondani, L.A., Nardelli, T.R., Nogueira, T.C., Esguerra, J.L.S., et al. (2017). Neuron-enriched RNA-binding proteins regulate pancreatic beta cell function and survival. J. Biol. Chem. *292*, 3466–3480. https://doi.org/10.1074/jbc.M116.748335.

89. Casteels, T., Bajew, S., Reiniš, J., Enders, L., Schuster, M., Fontaine, F., Müller, A.C., Wagner, B.K., Bock, C., and Kubicek, S. (2022). SMNDC1 links chromatin remodeling and splicing to regulate pancreatic hormone expression. Cell Rep. *40*, 111288. https://doi.org/10.1016/j.celrep.2022.111288.

90. Juan-Mateu, J., Bajew, S., Miret-Cuesta, M., Íñiguez, L.P., Lopez-Pascual, A., Bonnal, S., Atla, G., Bonàs-Guarch, S., Ferrer, J., Valcárcel, J., et al. (2023). Pancreatic microexons regulate islet function and glucose homeostasis. Nat. Metab. *5*, 219–236. https://doi.org/10.1038/s42255-022-00734-2.

91. Arntfield, M.E., and van der Kooy, D. (2011). β-Cell evolution: How the pancreas borrowed from the brain: The shared toolbox of genes expressed by neural and pancreatic endocrine cells may reflect their evolutionary relationship. BioEssays *33*, 582–587. https://doi.org/10.1002/bies.201100015.

92. van Arensbergen, J., García-Hurtado, J., Moran, I., Maestro, M.A., Xu, X., Van de Casteele, M., Skoudy, A.L., Palassini, M., Heimberg, H., and Ferrer, J. (2010). Derepression of Polycomb targets during pancreatic organogenesis allows insulin-producing beta-cells to adopt a neural gene activity program. Genome Res. *20*, 722–732. https://doi.org/10.1101/gr.101709.109.

93. Rogalska, M.E., Mancini, E., Bonnal, S., Gohr, A., Dunyak, B.M., Arecco, N., Smith, P.G., Vaillancourt, F.H., and Valcárcel, J. (2024). Transcriptome-wide splicing network reveals specialized regulatory functions of the core spliceosome. Science *386*, 551–560. https://doi.org/10.1126/science.adn8105.

94. Salz, H.K., and Erickson, J.W. (2010). Sex determination in Drosophila: The view from the top. Fly (Austin) *4*, 60–70. https://doi.org/10.4161/fly.4.1.11277.

95. Moschall, R., Rass, M., Rossbach, O., Lehmann, G., Kullmann, L., Eichner, N., Strauss, D., Meister, G., Schneuwly, S., Krahn, M.P., et al. (2019). Drosophila Sister-of-Sex-lethal reinforces a male-specific gene expression pattern by controlling Sex-lethal alternative splicing. Nucleic Acids Res. *47*, 2276–2288. https://doi.org/10.1093/nar/gky1284.

96. Raj, B., O'Hanlon, D., Vessey, J.P., Pan, Q., Ray, D., Buckley, N.J., Miller, F.D., and Blencowe, B.J. (2011). Cross-regulation between an alternative splicing activator and a transcription repressor controls neurogenesis. Mol. Cell *43*, 843–850. https://doi.org/10.1016/j.molcel.2011.08.014.

97. Li, H.Y., Bourdelas, A., Carron, C., and Shi, D.L. (2010). The RNA-binding protein Seb4/RBM24 is a direct target of MyoD and is required for myogenesis during Xenopus early development. Mech. Dev. *127*, 281–291. https://doi.org/10.1016/j.mod.2010.03.002.

98. Nogueira, T.C., Paula, F.M., Villate, O., Colli, M.L., Moura, R.F., Cunha, D.A., Marselli, L., Marchetti, P., Cnop, M., Julier, C., et al. (2013). GLIS3, a susceptibility gene for type 1 and type 2 diabetes, modulates pancreatic beta cell apoptosis via regulation of a splice variant of the BH3-only protein Bim. PLoS Genet. *9*, e1003532. https://doi.org/10.1371/journal.pgen.1003532.

99. Zhu, R., Li, X., Xu, J., Barrabi, C., Kekulandara, D., Woods, J., Chen, X., and Liu, M. (2019). Defective endoplasmic reticulum export causes proinsulin misfolding in pancreatic β cells. Mol. Cell. Endocrinol. *493*, 110470. https://doi.org/10.1016/j.mce.2019.110470.

100. Barrabi, C., Zhang, K., Liu, M., and Chen, X. (2023). Pancreatic beta cell ER export in health and diabetes. Front. Endocrinol. *14*, 1155779. https://doi.org/10.3389/fendo.2023.1155779.

101. Klochendler, A., Caspi, I., Corem, N., Moran, M., Friedlich, O., Elgavish, S., Nevo, Y., Helman, A., Glaser, B., Eden, A., et al. (2016). The genetic program of pancreatic β-cell replication in vivo. Diabetes *65*, 2081–2093. https://doi.org/10.2337/db16-0003.

102. Rogalska, M.E., Vivori, C., and Valcárcel, J. (2023). Regulation of pre-mRNA splicing: roles in physiology and disease, and therapeutic prospects. Nat. Rev. Genet. *24*, 251–269. https://doi.org/10.1038/s41576-022-00556-8.

103. Pasquali, L., Gaulton, K.J., Rodríguez-Seguí, S.A., Mularoni, L., Miguel-Escalada, I., Akerman, İ., Tena, J.J., Morán, I., Gómez-Marín, C., van de Bunt, M., et al. (2014). Pancreatic islet enhancer clusters enriched in type 2 diabetes risk-associated variants. Nat. Genet. *46*, 136–143. https://doi.org/10.1038/ng.2870.

104. Sanjana, N.E., Shalem, O., and Zhang, F. (2014). Improved vectors and genome-wide libraries for CRISPR screening. Nat. Methods *11*, 783–784. https://doi.org/10.1038/nmeth.3047.

105. Dull, T., Zufferey, R., Kelly, M., Mandel, R.J., Nguyen, M., Trono, D., and Naldini, L. (1998). A third-generation lentivirus vector with a conditional packaging system. J. Virol. *72*, 8463–8471. https://doi.org/10.1128/JVI.72.11.8463-8471.1998.

106. Miyazaki, J., Araki, K., Yamato, E., Ikegami, H., Asano, T., Shibasaki, Y., Oka, Y., and Yamamura, K. (1990). Establishment of a pancreatic beta cell line that retains glucose-inducible insulin secretion: special reference to expression of glucose transporter isoforms. Endocrinology *127*, 126–132. https://doi.org/10.1210/endo-127-1-126.

107. Dobin, A., Davis, C.A., Schlesinger, F., Drenkow, J., Zaleski, C., Jha, S., Batut, P., Chaisson, M., and Gingeras, T.R. (2013). STAR: ultrafast universal RNA-seq aligner. Bioinformatics *29*, 15–21. https://doi.org/10.1093/bioinformatics/bts635.

108. Patro, R., Duggal, G., Love, M.I., Irizarry, R.A., and Kingsford, C. (2017). Salmon provides fast and bias-aware quantification of transcript expression. Nat. Methods *14*, 417–419. https://doi.org/10.1038/nmeth.4197.

109. Love, M.I., Huber, W., and Anders, S. (2014). Moderated estimation of fold change and dispersion for RNA-seq data with DESeq2. Genome Biol. *15*, 550. https://doi.org/10.1186/s13059-014-0550-8.

110. Ramírez, F., Ryan, D.P., Grüning, B., Bhardwaj, V., Kilpert, F., Richter, A.S., Heyne, S., Dündar, F., and Manke, T. (2016). deepTools2: a next generation web server for deep-sequencing data analysis. Nucleic Acids Res. *44*, W160–W165. https://doi.org/10.1093/nar/gkw257.

111. Chen, E.Y., Tan, C.M., Kou, Y., Duan, Q., Wang, Z., Meirelles, G.V., Clark, N.R., and Ma'ayan, A. (2013). Enrichr: interactive and collaborative HTML5 gene list enrichment analysis tool. BMC Bioinformatics *14*, 128. https://doi.org/10.1186/1471-2105-14-128.

112. Kuleshov, M.V., Jones, M.R., Rouillard, A.D., Fernandez, N.F., Duan, Q., Wang, Z., Koplev, S., Jenkins, S.L., Jagodnik, K.M., Lachmann, A., et al. (2016). Enrichr: a comprehensive gene set enrichment analysis web server 2016 update. Nucleic Acids Res. *44*, W90–W97. https://doi.org/10.1093/nar/gkw377.

113. Zhou, Y., Zhou, B., Pache, L., Chang, M., Khodabakhshi, A.H., Tanaseichuk, O., Benner, C., and Chanda, S.K. (2019). Metascape provides a biologist-oriented resource for the analysis of systems-level datasets. Nat. Commun. *10*, 1523. https://doi.org/10.1038/s41467-019-09234-6.

114. Shannon, P., Markiel, A., Ozier, O., Baliga, N.S., Wang, J.T., Ramage, D., Amin, N., Schwikowski, B., and Ideker, T. (2003). Cytoscape: a software environment for integrated models of biomolecular interaction networks. Genome Res. *13*, 2498–2504. https://doi.org/10.1101/gr.1239303.

115. Subramanian, A., Tamayo, P., Mootha, V.K., Mukherjee, S., Ebert, B.L., Gillette, M.A., Paulovich, A., Pomeroy, S.L., Golub, T.R., Lander, E.S., et al. (2005). Gene set enrichment analysis: a knowledge-based approach for interpreting genome-wide expression profiles. Proc. Natl. Acad. Sci. USA *102*, 15545–15550. https://doi.org/10.1073/pnas.0506580102.

116. Park, J.W., Jung, S., Rouchka, E.C., Tseng, Y.T., and Xing, Y. (2016). rMAPS: RNA map analysis and plotting server for alternative exon regulation. Nucleic Acids Res. *44*, W333–W338. https://doi.org/10.1093/nar/gkw410.

117. Quinlan, A.R., and Hall, I.M. (2010). BEDTools: a flexible suite of utilities for comparing genomic features. Bioinformatics *26*, 841–842. https://doi.org/10.1093/bioinformatics/btq033.

118. Langmead, B., and Salzberg, S.L. (2012). Fast gapped-read alignment with Bowtie 2. Nat. Methods *9*, 357–359. https://doi.org/10.1038/nmeth.1923.

119. Li, H., Handsaker, B., Wysoker, A., Fennell, T., Ruan, J., Homer, N., Marth, G., Abecasis, G., and Durbin, R.; 1000 Genome Project Data Processing Subgroup (2009). The Sequence Alignment/Map format and SAMtools. Bioinformatics *25*, 2078–2079. https://doi.org/10.1093/bioinformatics/btp352.

120. Zhang, Y., Liu, T., Meyer, C.A., Eeckhoute, J., Johnson, D.S., Bernstein, B.E., Nusbaum, C., Myers, R.M., Brown, M., Li, W., et al. (2008). Model-based analysis of ChIP-seq (MACS). Genome Biol. *9*, R137. https://doi.org/10.1186/gb-2008-9-9-r137.

121. Heinz, S., Benner, C., Spann, N., Bertolino, E., Lin, Y.C., Laslo, P., Cheng, J.X., Murre, C., Singh, H., and Glass, C.K. (2010). Simple combinations of lineage-determining transcription factors prime cis-regulatory elements required for macrophage and B cell identities. Mol. Cell *38*, 576–589. https://doi.org/10.1016/j.molcel.2010.05.004.

122. Kulakovskiy, I.V., Vorontsov, I.E., Yevshin, I.S., Sharipov, R.N., Fedorova, A.D., Rumynskiy, E.I., Medvedeva, Y.A., Magana-Mora, A., Bajic, V.B., Papatsenko, D.A., et al. (2018). HOCOMOCO: towards a complete collection of transcription factor binding models for human and mouse via large-scale ChIP-seq analysis. Nucleic Acids Res. *46*, D252–D259. https://doi.org/10.1093/nar/gkx1106.

123. Wickham, H. (2009). Ggplot2: elegant graphics for data analysis. https://doi.org/10.1007/978-0-387-98141-3.

124. Reich, M., Liefeld, T., Gould, J., Lerner, J., Tamayo, P., and Mesirov, J.P. (2006). GenePattern 2.0. Nat. Genet. *38*, 500–501. https://doi.org/10.1038/ng0506-500.

125. Hao, Y., Stuart, T., Kowalski, M.H., Choudhary, S., Hoffman, P., Hartman, A., Srivastava, A., Molla, G., Madad, S., Fernandez-Granda, C., et al. (2024). Dictionary learning for integrative, multimodal and scalable single-cell analysis. Nat. Biotechnol. *42*, 293–304. https://doi.org/10.1038/s41587-023-01767-y.

126. Korsunsky, I., Millard, N., Fan, J., Slowikowski, K., Zhang, F., Wei, K., Baglaenko, Y., Brenner, M., Loh, P.R., and Raychaudhuri, S. (2019). Fast, sensitive and accurate integration of single-cell data with Harmony. Nat. Methods *16*, 1289–1296. https://doi.org/10.1038/s41592-019-0619-0.

127. Wang, L. (2021). Single-cell normalization and association testing unifying CRISPR screen and gene co-expression analyses with Normalisr. Nat. Commun. *12*, 6395. https://doi.org/10.1038/s41467-021-26682-1.

128. Shen, M., and Sinai, L. (2025). GeneOverlap: Test and visualize gene overlaps. https://doi.org/10.18129/B9.bioc.GeneOverlap.

129. Liu, B., Gloudemans, M.J., Rao, A.S., Ingelsson, E., and Montgomery, S.B. (2019). Abundant associations with gene expression complicate GWAS follow-up. Nat. Genet. *51*, 768–769. https://doi.org/10.1038/s41588-019-0404-0.

130. Myers, T.A., Chanock, S.J., and Machiela, M.J. (2020). LDlinkR: an R package for rapidly calculating linkage disequilibrium statistics in diverse populations. Front. Genet. *11*, 157. https://doi.org/10.3389/fgene.2020.00157.

131. Wallace, C. (2021). A more accurate method for colocalisation analysis allowing for multiple causal variants. PLoS Genet. *17*, e1009440. https://doi.org/10.1371/journal.pgen.1009440.

132. Schneider, C.A., Rasband, W.S., and Eliceiri, K.W. (2012). NIH Image to ImageJ: 25 years of image analysis. Nat. Methods *9*, 671–675. https://doi.org/10.1038/nmeth.2089.

133. Zhang, H., Fujitani, Y., Wright, C.V.E., and Gannon, M. (2005). Efficient recombination in pancreatic islets by a tamoxifen-inducible Cre-recombinase. Genesis *42*, 210–217. https://doi.org/10.1002/gene.20137.

134. Miguel-Escalada, I., Maestro, M.Á., Balboa, D., Elek, A., Bernal, A., Bernardo, E., Grau, V., García-Hurtado, J., Sebé-Pedrós, A., and Ferrer, J. (2022). Pancreas agenesis mutations disrupt a lead enhancer controlling a developmental enhancer cluster. Dev. Cell *57*, 1922–1936. e9. https://doi.org/10.1016/j.devcel.2022.07.014.

135. Balboa, D., Barsby, T., Lithovius, V., Saarimäki-Vire, J., Omar-Hmeadi, M., Dyachok, O., Montaser, H., Lund, P.E., Yang, M., Ibrahim, H., et al. (2022). Functional, metabolic and transcriptional maturation of human pancreatic islets derived from stem cells. Nat. Biotechnol. *40*, 1042–1055. https://doi.org/10.1038/s41587-022-01219-z.

136. Maestro, M.A., Boj, S.F., Luco, R.F., Pierreux, C.E., Cabedo, J., Servitja, J.M., German, M.S., Rousseau, G.G., Lemaigre, F.P., and Ferrer, J. (2003). Hnf6 and Tcf2 (MODY5) are linked in a gene network operating in a precursor cell domain of the embryonic pancreas. Hum. Mol. Genet. *12*, 3307–3314. https://doi.org/10.1093/hmg/ddg355.

137. Göpel, S., Kanno, T., Barg, S., Galvanovskis, J., and Rorsman, P. (1999). Voltage-gated and resting membrane currents recorded from B-cells in intact mouse pancreatic islets. J. Physiol. *521*, 717–728. https://doi.org/10.1111/j.1469-7793.1999.00717.x.

138. Briant, L.J.B., Zhang, Q., Vergari, E., Kellard, J.A., Rodriguez, B., Ashcroft, F.M., and Rorsman, P. (2017). Functional identification of islet cell types by electrophysiological fingerprinting. J. R. Soc. Interface *14*, 20160999. https://doi.org/10.1098/rsif.2016.0999.

139. Schmidl, C., Rendeiro, A.F., Sheffield, N.C., and Bock, C. (2015). ChIPmentation: fast, robust, low-input ChIP-seq for histones and transcription factors. Nat. Methods *12*, 963–965. https://doi.org/10.1038/nmeth.3542.

140. Pruim, R.J., Welch, R.P., Sanna, S., Teslovich, T.M., Chines, P.S., Gliedt, T.P., Boehnke, M., Abecasis, G.R., and Willer, C.J. (2010). LocusZoom: regional visualization of genome-wide association scan results. Bioinformatics *26*, 2336–2337. https://doi.org/10.1093/bioinformatics/btq419.

141. Maller, J.B., McVean, G., Byrnes, J., Vukcevic, D., Palin, K., Su, Z., Howson, J.M.M., Auton, A., Myers, S., et al.; Wellcome Trust Case Control Consortium (2012). Bayesian refinement of association signals for 14 loci in 3 common diseases. Nat. Genet. *44*, 1294–1301. https://doi.org/10.1038/ng.2435.

142. Wakefield, J. (2007). A Bayesian measure of the probability of false discovery in genetic epidemiology studies. Am. J. Hum. Genet. *81*, 208–227. https://doi.org/10.1086/519024.

STAR★METHODS

KEY RESOURCES TABLE

REAGENT or RESOURCE	SOURCE	IDENTIFIER
Antibodies		
Rat monoclonal anti-KRT19	DSHB	TROMA-III; RRID:AB_2133570
Rabbit monoclonal anti-HNF1α (D7z2Q)	Cell Signaling Technology	#89670; RRID:AB_2728751
Rabbit polyclonal anti-Glucagon	DAKO	A0565; RRID:AB_10013726
Guinea Pig polyclonal anti-Insulin	DAKO	A0564; RRID:AB_10013624
Rabbit polyclonal anti-A1CF – C-terminal region	Aviva System Biology	0AAB00687
Mouse monoclonal anti-E-Cadherin	BD Transduction Laboratories	#610181; RRID:AB_397580
Rabbit polyclonal H3 acetyl K27	Abcam	ab4729; RRID:AB_2118291
Rabbit monoclonal H3 trimethyl K4	Merck	04-745; RRID:AB_1163444
Mouse monoclonal anti-TBP	Abcam	Ab51841; RRID:AB_945758
Mouse monoclonal anti-HNF1A (F-7)	Santa Cruz	Sc-393925
Bacterial and virus strains		
LentiCRISPRv2	Sanjana et al.[104]	Addgene #52961
pMDLg/pRRE	Dull et al.[105]	Addgene #12251
pRSV-Rev	Dull et al.[105]	Addgene #12253
pMD2.G	Didier Trono Lab	Addgene #12259
Chemicals, peptides, and recombinant proteins		
L-Arginine	Merck	A5006
L-Arginine monohydrochloride	Merck	A5131
Ascorbid acid	Sigma	Cat# A4544
Nicotinamide	Sigma	Cat# N0636
Heparin	Sigma	Cat# H3149-25KU
Zinc Sulfate	Sigma	Cat# Z0251-100G
NaHCO3	Sigma	Cat# S5761
Glucose	SIGMA	Cat# G8769-100ML
BSA	Lampire	Cat# 7500804
Insulin-Transferrin-Selenium-Ethanolamine (ITS -X) (100X)	Life Technologies	Cat# 51500-056
Sodium pyruvate solution 100mM	Merck lifescience SLU	Cat# S8636-100ML
Chemically Defined Lipid Concentrate	Life Technologies	Cat# 11905031
Trace Elements A	Corning	Cat# 25-021-CI
Trace Elements B	Corning	Cat# 25-022-CI
GlutaMax	Life Technologies	Cat# 35050038
MCDB 131 Medium, no glutamine	Life Technologies	Cat# 10372-019
Corning CMRL 1066	Fisher Scientific	Cat# Corning 15-110-CV
Y-27632 2HCl (ROCKi)	Selleckchem	Cat# S1049
Matrigel Growth Factor Reduced	Corning	Cat# 356231
0.5 mM EDTA	ThermoFisher	Cat# 15575
FGF7	Genscript	Cat# Z03407-1
CHIR	Tocris	Cat# 4423
ActivinA	Qkine	Cat# QK001 ActA_1000
Human EGF	Peprotech	Cat# AF-100-15
Retinoic acid	Sigma	Cat# R2625
TPB (amyloid precursor protein modulator)	Santa Cruz Biotechnology	Cat# sc-204424

(*Continued on next page*)

Continued

REAGENT or RESOURCE	SOURCE	IDENTIFIER
SANT-1	Sigma	Cat# S4572
LDN-193189	Selleckchem	Cat# S2618
RepSox	Selleckchem	Cat# S7223
Human Betacellulin	Peprotech	Cat# 100-50-100UG
T3	Sigma	Cat# T6397-100MG
N-Acetyl Cysteine (NAC)	Sigma	Cat# A9165-5G
ZM447439	Selleckchem	Cat# S1103
Gamma Secretase Inhibitor XX (GSiXX)	Calbiochem	Cat# 565789
Exendin-4	Enzo	Cat# ENZ-PRT111-0001
Essential 8	Life Technologies	Cat# A1517001
Tamoxifen	Sigma-Aldrich	Cat# T5648
Critical commercial assays		
NEBuilder HiFi DNA Assembly Master Mix	New England Biolabs	E2621L
Ultra Sensitive Mouse Insulin ELISA Kit	Crystal Chem	#90080
Mouse Glucagon ELISA Kit	Crystal Chem	#81518
HTRF High Range Insulin Assay Kit	Revvity Health Sciences	#62IN1PEG
PEIpro	Polyplus-Transfection	101000017
RNAiMAX	Thermo Fisher	13778030
Quick-RNA Microprep Kit	Zymo Research	#R1050
Transcriptor First Strand cDNA Synthesis Kit	Roche	#4896866001
LightCycler 480 SYBR Green I Master	Roche	#4707516001
NucleoSpin Plus RNA kit	Cultek	872101
DirectPCR Lysis Reagent	Viagen Biotech	Cat#102-T
DreamTaq Green PCR Master Mix	Thermo Fisher Scientific	Cat#K1081
Phusion Green High-Fidelity DNA Polymerase	Thermo Fisher Scientific	Cat#F534S
Fluorescence Mounting Medium	Dako (now Agilent)	Cat#S3023
UltraPure Low Melting Point Agarose	Thermo Fisher Scientific	Cat# 16520050
NucleoSpin RNA Plus Kit	Macherey Nagel	Cat# 22740984.50
Transcriptor First Strand cDNA Synthesis Kit	Life Science Roche	Cat#04897030001
LightCycler 480 SYBR Green IMasterMix	Life Science Roche	Cat# 04707516001
Illumina Stranded Total RNA Library Prep kit	Illumina	20040534
Deposited data		
Raw and analysed (RNAseq)	This paper	GEO: GSE277551
Raw and analysed (ChIP-seq)	This paper	GEO: GSE277552
Experimental models: Cell lines		
Human pancreatic β-cell line EndoC-βH3	Philippe Ravassard lab	EndoC-βH3
Human embryonic stem cell line (hESC) H1	WiCell Research Institute	WA01
Human embryonic kidney 293 FT	Thermo Fisher	N/A
Mouse insulinoma cell line MIN6	Jun-ichi Miyazaki[106]	N/A
Experimental models: Organisms/strains		
Mouse / Strain: Alb Tg(Alb1-cre)1^{Khk}	Klaus Kaestner lab	MGI:2664969
Mouse / Strain: B6.Cg-Tg(Vil1-cre)997Gum/J	JAX	RRID:IMSR_JAX:004586
Mouse / Strain: B6.FVB-Tg(Pdx1-cre)6Tuv/J	JAX	RRID:IMSR_JAX:014647
Mouse / Strain: B6(Cg)-*Ins1*$^{tm1.1(cre)Thor}$/J	Ferrer lab	RRID:IMSR_JAX:026801
Mouse / Strain: B6;129S4-*Gcg*$^{em1(cre/ERT2)Khk}$/Mmjax	Klaus Kaestner lab	RRID:MMRRC_042277-JAX
Mouse / Strain: *Hnf1a LoxP*	Ferrer Lab	N/A
Mouse / Strain: *Tg(Pdx1-Cre/Esr1*)1Mga*	Maureen Gannon Lab	RRID:IMSR_JAX:037551
Mouse / Strain: *Hnf1a*$^{-/-}$	Frank Gonzalez Lab	N/A

(*Continued on next page*)

Continued

REAGENT or RESOURCE	SOURCE	IDENTIFIER
Oligonucleotides		
CRISPR genotyping sequence: HNF1A_KO: Fwd: CCTTCGCTAAGCACACGGAT / Rev: GGGCTCATGGGATTTGGGAC	This paper	N/A
CRISPR genotyping sequence: A1CF_KO: Fwd: TGTCACTGTCAAACCTGTTGGC / Rev: TCTGTGCACTAGGCTCATTTGC	This paper	N/A
A1CF ASO sequence: mU*mU*mG*mA*mA* T*T*C*C* T*T*T*T*C*A*mA*mU*mC*mA*mU	This paper	N/A
SLC7A2 SSO9.2 exon 7 block: mA*mC*mU*mC*mU*mC*mU*mC*mA*mC* mC*mU*mG*mC*mC*mA*mC*mU*mG*mC	This paper	N/A
SLC7A2 SSO9.3 exon 8 block: mU*mA*mA*mA*mG*mC*mU*mU*mA*mC* mC*mA*mG*mA*mA*mA*mU*mG*mA*mC	This paper	N/A
Scramble: mA*mA*mA*mU*mA*mA*mU*mU* mG*mA*mA*mU*mU*mU*mU*mA*mA*mA* mU*mA*mC*mG*mC*mU*mU	This paper	N/A
Guide RNA and qPCR oligonucleotides in Table S2	N/A	N/A
Recombinant DNA		
Lenti – CMV-HNF1A	This paper	Addgene #204379
Lenti – CMV-A1CF	This paper	Addgene #204377
Lenti – CMV-EGFP	This paper	Addgene #204387
Software and algorithms		
STAR (v2.7.10b & 2.7.11)	Dobin et al.[107]	N/A
Salmon (v1.9.0)	Patro et al.[108]	https://combine-lab.github.io/salmon/
Bioconductor R (v4.2.2) package DESeq2 (v1.38.0)	Love et al.[109]	https://www.bioconductor.org/
Deeptools (v3.5.1)	Ramirez et al.[110]	https://deeptools.readthedocs.io/en/develop/
Enrichr	Chen et al.[111] and Kuleshov et al.[112]	https://maayanlab.cloud/Enrichr/
Metascape	Zhou et al.[113]	https://metascape.org/gp/index.html#/main/step1
Cytoscape 3.10.2	Shannon et al.[114]	https://cytoscape.org/
GSEA Preranked tool	Subramanian et al.[115]	https://www.gsea-msigdb.org/gsea/index.jsp
rMATS (turbo v4.1.2 & 4.3.0)	Shen et al.[50]	https://rnaseq-mats.sourceforge.io/
rMAPS	Park et al.[116]	http://rmaps.cecsresearch.org/
bedtools (v2.13.3)	Quinlan and Hall[117]	https://bedtools.readthedocs.io/en/latest/
Bowtie2 (v2.1.0	Langmead and Salzberg[118]	https://bowtie-bio.sourceforge.net/bowtie2/index.shtml
Samtools (v1.2)	Li et al.[119]	https://www.htslib.org/
Picard (v2.6.0)	"Picard Toolkit." 2018. Broad Institute	http://broadinstitute.github.io/picard
MACS2 (v.2.1.0)	Zhang et al.[120]	N/A
HOMER (v4.10)	Heinz et al.[121]	http://homer.ucsd.edu/homer/download.html
HOCOMOCO	Kulakovskiy et al.[122]	https://hocomoco11.autosome.org/
ggplot2 R package	Wickham[123]	https://www.htslib.org/
GraphPad Prism 7	Graphpad	https://www.graphpad.com/features
Genepattern	Reich et al.[124]	https://www.genepattern.org/#gsc.tab=0
BioRender illustration software	BioRender	https://www.biorender.com/
GTEx Portal	GTEx consortium[74]	https://www.gtexportal.org/home/
Seurat 5.0.1	Hao et al.[125]	https://satijalab.org/seurat/

(*Continued on next page*)

Continued

REAGENT or RESOURCE	SOURCE	IDENTIFIER
Harmony	Korsunsky et al.[126]	https://portals.broadinstitute.org/harmony/
Normalisr	Wang et al.[127]	https://github.com/lingfeiwang/normalisr
GeneOverlap R package	Shen and Sinai[128]	https://bioconductor.org/packages/GeneOverlap
LocusCompareR 1.0.0	Liu et al.[129]	http://locuscompare.com/
LDlinkR package for R	Myers et al.[130]	https://cran.r-project.org/web/packages/LDlinkR/vignettes/LDlinkR.html
FUSION	Gusev et al.[70]	http://gusevlab.org/projects/fusion/
COLOC	Wallace[131]	https://chr1swallace.github.io/coloc/
ImageJ	Schneider et al.[132]	https://imagej.net/ij/
Other		
Infinite M200 plate reader	Tecan	N/A
MZ16F stereomicroscope	Leica	N/A
SP5 confocal microscope	Leica	N/A
NEPA21 Super Electroporator	Nepagene	N/A
LightCycler 480 Instrument II	Roche	N/A
Bioanalyzer	Agilent	N/A
Islet perifusion chamber	BIOREP Technologies	Cat#PERI-CHAMBER
Perifusion chamber filter	BIOREP Technologies	Cat#PERI-FILTER
Perifusion chamber rubber ring	BIOREP Technologies	Cat#PERI-O-RING
Perifusion steel nozzle	BIOREP Technologies	Cat#PERI-NOZZLE
8-channel peristaltic pump	ISMATEC	Cat#ISM931A
Two-stop color code tube 0.38mm ID Tygon R3607	ISMATEC	Cat#070534-03i / SC0003
Connecting tube 1.016mm ID Tygon 3603	ISMATEC	Cat#SC0035

EXPERIMENTAL MODEL AND SUBJECT DETAILS

Animal studies

Animal experimentation complies with EU Directive 86/609/EEC and Recommendation 2007/526/EC regarding the protection of animals used for experimental and other scientific purposes, enacted under Spanish law 1201/2005. All experiments were approved by the Institutional Animal Care Committees of the University of Barcelona and Parc de Recerca Biomedica de Barcelona. The *Hnf1a* exon 2 floxed allele was described.[16] Cre-mediated excision of exon 2 removes amino acid residues 109-174 in the DNA binding domain (which spans residues 87-279) and results in a premature stop codon. In consequence, the excised allele eliminates HNF1A residues 109-628, including most of the DNA binding domain and all transactivation domains. The Hnf1a$^{-/-}$,[10] *Alb-Cre*[32] (also known as *Albafp*-Cre), *Vil1-Cre*,[34] *Pdx1-Cre*,[35] *Ins1-Cre*,[41] *Gcg-CreERT*[2,40] and *Pdx1-CreER*[133] mouse lines have been previously described.

All animals were housed in a pathogen barrier-sustained environment, in individually ventilated cages, a 12-hour light cycle, controlled relative humidity (40—60%) and temperature (24°C). Cage bedding, food, and water were provided ad libitum. The experiments were carried out using littermates of same sex. Animal tissue collection was performed on anesthetized animals using isoflurane (Zoetis) prior to decapitation. For histology assessment, tissues were fixed in 4% paraformaldehyde (Sigma-Aldrich) before paraffin embedding. For *Alb-Cre*, *Vil1-Cre*, *Pdx1-Cre*, *Ins1-Cre*, mouse strains without *Hnf1a* floxed alleles and expressing Cre recombinase were used as controls, for inducible Cre lines (*Gcg*^{CreERT2} and *Pdx1*^{CreER}) *Hnf1a* floxed mice without Cre treated with tamoxifen were used as controls. Only littermate male mice were used for comparisons.

Human embryonic kidney 293 FT (HEK293FT)

HEK293FT cells for lentivirus production were cultured in Dulbecco's Modified Eagle Medium (DMEM) High Glucose (Gibco, #41965039), supplemented with 10% FBS (Life Technologies, #10270-106), 1% GlutaMAX (Life Technologies, #35050-038), 1 mM sodium pyruvate (Sigma, #S8636) and 0.1 mM non-essential amino acids (Corning, #25-025-CI).

MIN6

MIN6 cells were cultured in DMEM High Glucose (Gibco, #41965039) supplemented with 15% FBS (Life Technologies, #10270-106), 1% GlutaMAX (Life Technologies, #35050-038), 1% Penicillin-Streptomycin (Life Technologies, #15140122) and 2.5 μl β-mercaptoethanol (Sigma M3148-25ML).

Generation of EndoC-βH3 mutant models

The human pancreatic β-cell line EndoC-βH3[42] was cultured in Advanced DMEM/F12 (Thermo Fisher Scientific, #12634-010) supplemented with 2% fatty acid-free Bovine Serum Albumin Fraction V (Roche, #10775835001), 6.7 ng/mL sodium selenite (Sigma, #S5261), 50 μM 2-mercaptoethanol (Sigma, #M3148), 5.5 μg/mL human transferrin (Sigma, #T8158-1G), 10 mM nicotinamide (Sigma, #N0636), 1% GlutaMAX and 100 U/mL Penicillin-Streptomycin (Life Technologies, #15140122). Plates were coated with DMEM High Glucose and 1% Extracellular Matrix Gel from Engelbreth-Holm-Swarm murine sarcoma (Sigma, #E1270) and 2 μg/mL fibronectin from bovine plasma (Sigma, #F1141) for 1 h at 37°C. *HNF1A*, *A1CF* mutant EndoC-βH3 cells were generated using CRISPR-Cas9 ribonucleoproteins. (Alt-R S.p. HiFi Cas9 Nuclease V3, 77522245, Integrated DNA Technologies (IDT). Two guide RNAs (Table S2) targeting a coding exon (exon 1 and 11 in *HNF1A*^{KO} and *A1CF*^{KO}, respectively) of the gene of interest were designed using Benchling (Biology Software, 2019) and Custom Alt-R CRISPR-Cas9 guide RNA (IDT), synthesized as crRNA and complexed with tracrRNA (Alt-R CRISPR-Cas9 tracrRNA, ATTO 550, 1075928, IDT). Ribonucleoprotein complexes were prepared according to manufacturer's instructions and electroporated into EndoC-βH3 (NEPA21 Super Electroporator, Nepagene). Electroporated cells were plated, expanded and single cell cloned using limited dilution. Resulting clones were expanded, processed for DNA extraction with DirectPCR Lysis Reagent (Viagen Biotech) and genotyped for deletions using PCR with Phusion High-Fidelity DNA polymerase (Genotyping primer sequences described in Table S2). We were not able to establish *HNF1A*^{KO} EndoC-βH3 clones, and therefore pools of CRISPR-Cas9 RNPs treated cells 5 days after electroporation were used instead.

Generation and differentiation of stem cell models

Experiments on human embryonic stem cells received authorization from the Health Department, Generalitat de Catalunya (register number 0336/2443/2019), subsequent to ethical and methodological approval by Center of Regenerative Medicine in Barcelona and the Institute of Health Carlos III (Ministry of Science and Innovation), ensuring compliance with European and National standards. Human embryonic stem cell line (hESC) H1 (WA01) was obtained from WiCell Research Institute and cultured on plates coated with 45 μg/mL Growth Factor Reduced Matrigel (Corning, #356231). Culture medium Essential8 (E8) (Life Technologies; A1517001) was changed every 24 or 48 hours depending on cell culture density. Cells were passaged with 0.5 mM EDTA (Life Technologies; 15575-038) in PBS. ROCK inhibitor Y-27632 2HCL (Selleckchem, #S1049) was used at 5–10 μM upon thawing. *HNF1A*^{KO} and *A1CF*^{KO} H1 cells were generated using CRISPR-Cas9 ribonucleoproteins targeting their coding exons, 1 and 11, respectively (Table S2) as described before.[45,134] Briefly, homozygous deletions were generated using two guide RNA flanking the coding exon designed using Bechling (Biology Software, 2019). Custom Alt-R CRISPR-Cas9 guide RNA (IDT), synthesized as crRNA, were complexed with tracrRNA (Alt-R CRISPR-Cas9 tracrRNA, ATTO 550, 1075928, IDT) and SpCas9 protein (Alt-R S.p. HiFi Cas9 Nuclease V3, 77522245, Integrated DNA Technologies (IDT) according to manufacturer instructions. Ribonucleoprotein complexes were electroporated delivered to one million stem cells (NEPA21 Super Electroporator, Nepagene). Electroporated cells were cultured, expanded and single cell cloned using single cell sorting to 96-well plates. Single cell-derived stem cell clones were screened for homozygous deletions using PCR with primers flanking the expected deletion (Table S2). Three *HNF1A*^{KO} and three *A1CF*^{KO} H1 homozygous deletion clonal cell lines were used for differentiation experiments, together with control clonal cell lines generated with non-targeting gRNAs previously described and the parental unmodified H1 cell line.[45,134] KO and control cells were differentiated to pancreatic islets (SC-islets) as described.[135] Differentiations were prepared by dissociating stem cells to single cells using 10 min incubation with 5 mM EDTA and seeding them at 0.22 million cells/cm2 onto Matrigel coated plates containing E8 medium with 5 μM ROCK inhibitor. The day after, differentiation was started following a seven-stage differentiation protocol: (1) Definitive endoderm induction (3 days): MCDB131 (Life Technologies, #10372-019) + 2 mM Glutamax (Life Technologies, #35050038) + 1.5 g/L NaHCO3 (Biowest, P2060) + 0.5% BSA fraction V Fatty acid free (Sigma-Aldrich, #A7030) + 10 mM final glucose (Sigma-Aldrich, #G8769) + 100 ng/ml Activin A (Qkine, #QK001) + 3 μM CHIR 99021 (Tocris, #4423). CHIR concentration decreased to 0.3 μM on day 1and 0 μM on day 2. (2) Posterior foregut induction (3 days): MCDB131 + 2 mM Glutamax + 1.5 g/L NaHCO3 + 0.5% BSA + 10 mM final glucose + 0.25 mM Ascorbic acid (Sigma-Aldrich, #A4544) + 50 ng/mL FGF7 (Genscript, #Z03047). (3) Pancreatic endoderm induction (2 days): MCDB131 + 2 mM Glutamax + 2.5 g/L NaHCO3 + 2% BSA + 10 mM final glucose + 1:200 ITSX (Life Technologies, #51500-056) + 0.25 mM Ascorbic acid + 50 ng/mL FGF7 + 0.25 μM SANT1 (Sigma-Aldrich, #S4572) + 1 μM Retinoic Acid (RA) (Sigma-Aldrich, #R2625) + 100 nM LDN-193189 (Selleckchem, #S2618), + 200 nM TPB (Santa Cruz Biotechnology, #sc-204424). (4) Pancreatic progenitor induction (4 days): MCDB131 + 2 mM Glutamax + 2.5 g/L NaHCO3 + 2% BSA + 10 mM final glucose + 1:200 ITSX + 0.25 mM Ascorbic acid + 2 ng/mL FGF7 + 0.25 μM SANT1 + 0.1 μM RA + 200 nM LDN-193189 + 100 nM TPB + 100 ng/mL EGF (Peprotech, AF-100-15) + 10 mM Nicotinamide (Sigma-Aldrich, N0636) + 10 ng/mL Activin A + 10 μM ROCKi. On day 2 of stage 4, cells were dissociated and reaggregated in 6-well aggrewell plate (StemCell Technologies, #34425) for 2 days. After that, aggregates were cultured in suspension in a rotating platform (InforsHT, Celltron) at 95 rpm. (5) Endocrine progenitor induction (4 days): MCDB131 + 2 mM Glutamax + 1.5 g/L NaHCO3 + 2% BSA + 20 mM final Glucose + 1:200 ITSX + 10 μg/mL Heparin (Sigma-Aldrich, #H3149) + 10 μM Zinc Sulfate (Sigma-Aldrich, #Z0251) + 0.25 μM SANT1 + 0.05 μM RA + 100 nM LDN-193189 + 10 μM ALK5inhII (Selleckchem, #S7233) + 1 μM GC1 (Tocris, #4554) + 20 ng/mL Betacellulin (Peprotech, #100-50) + 100 nM GSiXX (Millipore, #565789). (6) Endocrine cell induction (8 days): MCDB131 + 2 mM Glutamax + 1.5 g/L NaHCO3 + 2% BSA + 20 mM final glucose + 1:200 ITSX + 10 μg/mL Heparin + 10 μM Zinc Sulfate + 100 nM LDN-193189 + 10 μM ALK5inhII + 1 μM GC1 + 100 nM GSiXX. (7) Endocrine cell maturation (21 to 35 days): Corning CMRL 1066 (Cultek, #5515-110-CV) + 2 mM Glutamax + 2% BSA fV + 1:200 ITSX + 10 μg/mL Heparin + 0.5 mM Sodium pyruvate (Merck, #S8636) + 10 μM Zinc Sulfate + 1:2000 Lipid concentrate (Life Technologies, #11905031)+ 1:2000 Trace elements A (Corning,

#25-021-CI) + 1:2000 Trace elements B (Corning, #25-022-CI) + 1 mM N-Acetyl-Cysteine (Sigma-Aldrich, #A9165) + 10 nM Tri-iodothyronine (T3) (Merck, #T6397) + ZM447439 (Selleckchem, #S1103).

METHOD DETAILS

General cell culture methods

All cells were cultured at 37°C and 5% CO_2 in a humidified incubator. All cell culture media were filtered using 0.22 μM polyvinylidene difluoride (PVDF) filters (Stericup 500 mL filter, Millipore #S2GPU05RE) prior to use.

Mouse pancreatic islet isolation

Cold collagenase P (Roche) at 1 mg/ml in Hank's Balanced Salt Solution (HBSS) was perfused to the pancreas through the main duct. The pancreas was digested at 37°C for 10 min in agitation, gently disaggregated using a needle and washed with cold HBSS 0.5% bovine albumin serum (BSA). Disaggregated pancreas was suspended in 7 ml of a mixture of room temperature Histopaque 1077 and 1119 (Merck) at a ratio of 7:3, then 7ml of HBSS 0.5% BSA was gently layered on top and centrifuged at 950 rcf for 20 min with no brake at RT. The interphase containing the islets was collected and washed in HBSS 0.5% BSA. Islets were further selected using a stereomicroscope and cultured for 1-2 days in RPMI with 10% FBS and Pen-Strep (1:100) at 37°C and 5% CO_2.

Glucose homeostasis studies

Mice were fasted overnight and received intraperitoneal injection (ipGTT) or oral gavage (oGTT) of glucose at (2 g/Kg). For insulin sensitivity assessment, mice were starved for 4h, received an injection of insulin (ipITT) at 0.75 U/kg. Arginine challenge was performed by infusing 5 mmol/Kg of arginine by gavage. Basal glycemia was measured before injection or gavage and 15, 30, 60 and 120 min post glucose, insulin or arginine administration. Blood was also collected on EDTA collection tubes (Sarstedt). For meal-tests, mice were fasted overnight and glycemia was measured before and 1h post refeeding. Serum was collected for insulin or glucagon measurement. Plasma insulin and glucagon were measured using Ultra Sensitive Mouse Insulin ELISA Kit (Crystal Chem #90080) or Mouse Glucagon ELISA Kit (Crystal Chem #81518) respectively, following manufacturers protocol. For plate reading an Infinite M Plex (Tecan) spectrophotometer was used.

Immunofluorescence staining

Murine tissues and SC-islets were fixed in 4% paraformaldehyde overnight at 4°C, SC-islets were stained with eosin before embedding in low-melting agarose (Sigma, #A9414), both murine and SC-islets were then embedded in paraffin blocks. Immunofluorescence staining was performed as previously described.[136] Briefly, paraffin blocks were cut in 4 μm sections, deparaffinized with xylene and rehydrated following decreasing ethanol concentrations. Sections were boiled for antigen unmasking in 10 mM citrate buffer pH 6 for 10 min, and permeabilized with 0.5% Triton X-100 (Sigma) PBS solution. Blocking was performed with antibody diluent (DAKO corporation) with 3% normal donkey serum for 1h in humid chamber. Slides were incubated with primary antibody (Table S1) at 4°C in humid chamber overnight. Slides were then incubated with secondary antibodies for 1 h in humid chamber at RT, washed for 5 min in PBS 0.2% Triton X-100 and mounted using fluorescence mounting medium (DAKO). Images were acquired with a confocal scanning microscope (Leica SPE).

β-cell area quantification

To quantify relative β-cell area, we analyzed pancreas from 5 *Hnf1a*^{WT} and 5 *Hnf1a*^{pKO} adult mice. Paraffin-embedded blocks were used to obtain 8 sections separated by >160 μm. After insulin, glucagon and DAPI co-staining, an image of the entire pancreatic section was captured, reconstructing a mosaic image taken with a 5x objective using the Zeiss Cell Observer fluorescence microscope. The three resulting channels were separated and brought to saturation to define areas for quantification. To further define the pancreatic area used as a denominator, we manually demarcated the pancreatic area, erasing lymph nodes, mesenteric fat remnants and artifacts such as auto-fluorescent microfibers, attempting to retain all other intraparenchymal cells. All areas (insulin, glucagon, and total pancreatic area) were quantified with Measure (ImageJ), after threshold definition. An alternate analysis was also performed in which areas occupied by infiltrating intrapancreatic adipocyte-like cells were omitted from the full pancreatic area used as a denominator, which also yielded non-significant differences between groups.

Lentivirus production and transduction of EndoC-βH3 and SC-islets

A lentiviral backbone for the overexpression of cDNAs was generated from LentiCRISPRv2 vector (Addgene #52961). Using Gibson assembly (NEBuilder HiFi DNA Assembly Master Mix, E2621L), we first replaced the vector promoter by CMV promoter and then cloned the cDNA of HNF1A, A1CF and EGFP amplified from SC-islet retrotranscribed DNA. These plasmids have been deposited on Addgene (#204379, #204377, #204387). Third generation lentiviral packaging plasmids pMDLg/pRRE, pRSV-Rev and pMD2.G (Addgene #12251, 12253 and 12259, respectively) together with the plasmid of interest or transfer plasmid were transfected into HEK293FT cells using PEIpro reagent (Polyplus-Transfection). Culture medium was replaced the following day and virus-containing medium was collected at day 3 post-transfection. Lentiviral particles were concentrated ~150 times by using Lenti-X Concentrator (Takara). EndoC-βH3 were plated onto 24-well plates, and transduced with concentrated lentiviral particles using 10 μg/mL polybrene (Merck, #TR-1003-G). Medium was replaced 48 h after transduction. SC-islets were collected in 15mL Falcons, and dispersed

to single cells using a 1:1 solution of TrypLE (Life Technologies, #12563029) and Trypsin-EDTA (0.05%) (ThermoFisher, #25300054) for approximately 8 min at 37 °C in a water bath. TrypLE-Trypsin was inactivated with 5% FBS in PBS and dissociated cells were centrifuged for 5 min at 250 rcf. Cells were resuspended in medium at a concentration of 2 million cells/mL. One million single cells per genotype, replicate and condition were transduced with ~1.5x10^9 viral genome copies, and polybrene (Merck, #TR-1003-G) was added to a final concentration of 10 μg/mL. Spin-infection was performed for 90 min at 900 rcf at 37 °C in 24-well ultra-low attachment plates (Corning, #153473). Next, transduced single cells were transferred to a 24-well aggrewell plate (StemCell Technologies, #34415) to induce reaggregation into SC-islet-like clusters or pseudoislets. Two days post-transduction, pseudoislets were put in suspension culture using 6-well ultra-low attachment plates, and medium was replaced. Six days post-transduction, cells were collected for RNA extraction or insulin release studies.

SSO and ASO experiments

EndoC-βH3 were plated onto 24-well plates, expanded and transfected using Lipofectamine RNAiMAX (Thermo Fisher, 13778030). ASO and SSO oligos (see Table S2) were purchased from Integrated DNA Technologies (IDT), resuspended in TE buffer at 1 mM, and complexed with Lipofectamine RNAiMAX following manufacturer's instructions. A final concentration of 50 nM was used to reverse transfect 300 000 Endoc-βH3 cells plated in a well of a 24-well plate. Transfection reagents-containing media was removed 24 hours after plating and samples were collected for RNA isolation and RT-qPCR analysis 72 hours post-transfection.

In vitro insulin secretion studies

Dynamic perifusion system was performed using an in-house system, Ismatec 8-channel peristaltic pump (Ismatec ISM931A), 2-stop 0.38 mm tygon tubes (Fisher Scientific) connected to a perifusion chamber (Biorep PERI-CHAMBER) and to 1.016 mm tygon tube (Fisher Scientific) connected to steel nozzle for consistent drop collection was used (Biorep PERI-NOZZLE). 100 primary islets or SC-islets were loaded in a fiberglass filter (Biorep PERI-FILTER) and 37°C Krebs Ringer Buffer (KRB) with different glucose concentrations and secretagogues at a fixed flow of 150 ul/min was perfused and effluent was manually collected every 5 minutes in 96 deep-well plates. For total insulin content measure, islets were recovered after the experiment, sonicated for 25 seconds in water and an aliquot transferred to acidic ethanol (1.5% HCl in 100% ethanol). Static insulin release analysis was performed as follows: 50 SC-islets or 300000 EndoC-βH3 cells per 12-well or 24-well plate wells respectively were pre-incubated in 1ml of KRB with 3mM of glucose for 1 h at 37°C, then washed with KRB with no glucose, and then subsequently incubated for 30 min with different glucose concentrations and/or secretagogues at 37°C. Finally, SC-islets or EndoC-βH3 were collected for insulin content measurement as done in dynamic insulin release studies. Insulin was measured using Cisbio HTRF High Range Insulin Assay Kit (Cisbio # 62IN1PEG) following manufacturers instructions, and read in a SPARK 10M multimode plate reader (Tecan).

Electrophysiological recordings of mouse islets

For electrophysiology, islets from control (*Hnf1a*^{WT}) and Hnf1a-deficient (*Hnf1a*^{iPanKO}) mice were isolated in Barcelona shipped overnight to Gothenburg prior to experiments. Upon receipt, islets were allowed to recover for at least 2 h before the recordings. The membrane potential of β-cells in intact islets was measured in the current-clamp mode using the perforated patch whole-cell technique, which retains intracellular metabolism, as previously described.[137] Islets were perfused with an extracellular solution and the temperature was kept at ~34°C. For current clamp recordings, the extracellular solution contained (mM) 140 NaCl, 3.6 KCl, 0.5 $MgSO_4$, 1.3 $CaCl_2$, 5 $NaHCO_3$, 0.5 NaH_2PO_4 and 10 HEPES (pH 7.4 using NaOH). The intracellular solution contained (mM) 76 K_2SO_4, 10 KCl, 10 NaCl, 1 $MgCl_2$ and 5 HEPES (pH 7.15 with KOH). Insulin-producing b-cells were identified by the electrophysiological fingerprint.[138]

RNA extraction

Total RNA from pancreatic islets, EndoC-βH3 or SC-islets was isolated using NucleoSpin Plus RNA kit (Cultek, @22740984.5) according to manufacturer's protocol or when input material was scarce, such as for transduced SC-islets or EndoC-βH3 cells, RNA was extracted using Quick-RNA Microprep Kit (Zymo Research, #R1050). Nanodrop (ThermoFisher) swas used to measure RNA quality and concentration.

Quantitative PCR (qPCR)

From 0.3 to 1 μg RNA, depending on the experiment and sample abundance, were denatured at 65°C for 10 min with 1μL Anchored Oligo (dT)18 Primer from Transcriptor First Strand cDNA Synthesis Kit (Roche, #4896866001) and kept on ice. Reverse transcription (RT) was performed with 4μL of Reaction buffer, 2μL of Deoxynucleotide mix, 0.5μL Protector RNAse inhibitor and 0.5μL Reverse transcriptase in a thermocycler: 60 min at 50°C, 5 min at 85°C, hold at 4°C. qPCR reactions were prepared with 7.5-12.5 ng of retrotranscribed RNA (cDNA), and were amplified with 2.5 μL of forward and reverse primer mix at 2 μM each using 5 uL of 2X LightCycler 480 SYBR Green I Master (Roche, #4707516001) in a final volume of 10μL. 384 plates (VWR, #731-0164P) were loaded into a LightCycler 480 Instrument II (Roche) with a thermal cycle of 95°C for 10 min, followed by 45 cycles of 95°C, 20s; 60°C, 20 s; 72°C, 20s, plus a melting step (95°C, 30s; 68°C, 60s; ramp at 0.05°C/s and 98°C, 15s). Relative quantification of gene expression was analysed with the ΔΔCt method. *TBP* or *CYCLOG* were used as housekeeping genes for normalizing gene expression and a

control cDNA sample from the same cell type was used as calibrator across all qPCR plates from the same experiment. RT-reaction products without RNA template and qPCR mix without any cDNA were used as negative controls. The oligonucleotides used for qPCR areshown in Table S2.

RNA-seq and differential gene expression

RNA from mouse islets or EndoC-βH3 mutant cells was quantified with Qubit (Thermo Fisher Scientific) and verified with Bioanalyzer (Agilent). Libraries were prepared from 300 ng RNA using Illumina Stranded Total RNA Library Prep kit and sequenced on a NovaSeq6000 (2x150 bp reads, flowcell S2, 50 M reads / sample). RNA-seq reads were aligned to the mouse (GRCm38.p6 v. M24) or human (GRCh38 gencode v.42) transcriptomes using STAR (v2.7.10b)[107] and Salmon (v1.9.0).[108] Salmon quant files were employed to identify genes differentially expressed (DE) between mutant and WT/Control samples (FDR < 0.05; 0.585 < Log2 fold change < -0.585) using Bioconductor R (v4.2.2) package DESeq2 (v1.38.0).[109] For RNA-seq track visualization, STAR was used to generate BAM files that were subsequently converted into bigwig files with Deeptools (v3.5.1).[110]

Western blotting

Stage 7 SC-islets were dissociated with TrypLE for 7 min at 37 °C, and then cells were lysed with hypotonic lysis buffer (100 mM HEPES pH 7.9, 15 mM MgCl2, 100 mM KCl). Nuclei were released using 0.6% NP-40 (Merck, #I8896) and centrifuged to separate the fraction containing cytoplasmic proteins. Nuclei pellet was lysed with nuclear lysis buffer (50 mM Tri-HCl pH 8, 150 mM NaCl, 0.5% NP-40) and vigorous agitation (30 min at 4°C). Nuclear and cytosolic protein extracts were snap-frozen and stored at -80°C. Quantification was performed using Pierce BCA Protein Assay Kit according to manufacturer's instructions (Fisher Scientific, #10678484). Electrophoresis was performed by loading 30 μg protein on NuPAGE 10% Bis-Tris Mini Protein Gel (Fisher Scientific, #10063412) with NuPAGE MOPS SDS running buffer (Fisher Scientific, #11589156). Samples were transferred into a PVDF membrane using NuPAGEtrade transfer buffer (Fisher Scientific, #11539166), and membrane blocking was performed using 5% non-fat dry milk in TBS-0.1% Tween 20 (Sigma, #P9416). Primary antibodies were incubated overnight at 4 °C: rabbit anti-HNF1A clone D7Z2Q (1/1000; Cell Signaling, #89670) and mouse anti-TBP (Abcam, #ab51841). Secondary antibodies were incubated for 1 h at room temperature: anti-rabbit IgG HRP-linked (1/2,000; Cell Signaling, #7074S) and anti-mouse IgG HRP-linked (1/2,000; Cell Signaling, #7076S). HRP was detected using Immobilon Western Chemiluminiscent HRP substrate (Merck Millipore, #WBKLS0100) and iBright Western Imager (ThermoFisher Scientific) to visualize the protein bands.

Functional enrichment analysis

Functional enrichment analysis was performed with Enrichr,[111,112] Metascape,[113] and gene set enrichment analysis using the GSEA Preranked tool.[115] Functional annotation network was performed with Cytoscape 3.10.2.

Differential alternative splicing

RNA-seq reads were aligned to the mouse (GRCm38.p6 v.M24) and human (GRCh38 gencode v.42) genomes using STAR. Differential alternative splicing events between the distinct *HNF1A* and *A1CF*-deficient models and their respective controls were identified with rMATS (turbo v4.1.2)[50] using default settings. Alternative splicing events with FDR < 0.05 and absolute delta (Δ) percent-spliced-in (Psi) > 0.1 were considered significant. In addition, only AS events with at least 10 reads in any of the samples (KO or control) were retained for further analysis. Alternative splicing events were classified into predefined categories by rMATS, and SE events were divided into EI (exon inclusion) and ES (exon skipping) events. Common splicing events between EndoC-βH3 $HNF1A^{KO}$ and $A1CF^{KO}$ were obtained by overlapping event genomic coordinates using bedtools (v2.13.3)[117] intersect tool with the -woparameter (an overlap of at least 1bp was considered an intersection).

ChIP-seq

ChIP experiments were performed on ∼5 million EndoC-βH3 or MIN6 cells. Cells were washed in cold 1x PBS with protease inhibitors and then crosslinked in 1% formaldehyde for 10 min at RT in rotation. After quenching in 0.125 M glycine for 5 min, cells were washed in PBS and lysed in ChIP lysis buffer (2% Triton X-100, 1% SDS, 100 mM NaCl, 10 mM Tris-HCl pH 8.0, 1 mM EDTA and protease inhibitors) on ice for 30 min. Chromatin lysate was sonicated for 8 min (aiming for fragments between 150-400 bp) using a S220 Focused Ultrasonicator (Covaris) with the following settings: duty cycle 2%, peak incident power 105 W, cycles per burst 200. Chromatin was centrifuged at max speed for 5 min at 4°C to remove debris and diluted 5 times with ChIP dilution buffer (50 mM Hepes pH 8.0, 140 mM NaCl, 1 mM EDTA, 0.75% Triton X-100, 0.1% Na-deoxycholate and protease inhibitors). Chromatin was pre-cleared with 20 μl of Dynabeads Protein G (Thermo Fisher) and then incubated in ChIP working buffer (1 part of ChIP lysis buffer and 4 parts of ChIP dilution buffer) with HNF1A, H3K4me3 and H3K27ac antibodies (1:50) (key resources table) and 0.5% BSA ON at 4°C with rotation. Dynabeads Protein G were also blocked ON in ChIP working buffer plus 0.5% BSA. The following day, immune complexes were pulled down with 30 μl of blocked beads for 2-3 hours. From this point forward, the ChIPmentation procedure[139] was performed. Briefly, beads were subsequently washed twice with RIPA-LS (10 mM Tris-HCl, pH 8.0, 140 mM NaCl, 1mM EDTA, pH 8.0, 0.1% SDS, 0.1% Na-Deoxycholate, 1% Triton X-100), RIPA-HS (10 mM Tris-HCl, pH 8.0, 500 mM NaCl, 1mM EDTA, pH 8.0, 0.1% SDS, 0.1% Na-Deoxycholate, 1% Triton X-100), RIPA-LiCl (10 mM Tris-HCl, pH 8.0, 250 mM LiCl, 1mM EDTA, pH 8.0, 0.5% IGEPAL, 0.5% Na-Deoxycholate) and once with 10 mM Tris pH 8.0. Chromatin was tagmented using 1 μl of the Tagment DNA Enzyme from the Nextera DNA Sample Prep Kit (Illumina) at 37°C for 10 min followed by two washes with RIPA-LS and TE. Then

DNA was de-crosslinked in ChIP elution buffer (10mM Tris-HCL pH 8.0, 5mM EDTA pH 8.0, 300mM NaCl and 0.4% SDS) with proteinase K at 55°C for 1 hour and 65°C ON, and finally purified using the MinElute PCR Purification Kit (QIAGEN). Libraries were amplified by PCR (number of cycles were determined by qPCR using the Ct + 1 value) with KAPA HiFi Hotstart Ready mix (Kapa Biosystems) and size-selected (250–350 bp) employing Agencourt AMPure XP beads (Beckman Coulter). Bioanalyzer was used for sample QC and library pooling for multiplexing. ChIP-seq libraries were sequenced in an Illumina NextSeq system with single-end reads of 75 bp aiming for ~30 million reads per sample.

ChIP-seq reads were processed as follows: i) alignment to the mouse (mm10) or human (hg19) genome using Bowtie2 (v2.1.0)[118]; ii) creation of bam files filtering for multi-mapping (min MAPQ = 30) by Samtools (v1.2)[119]; iii) removal of duplicate reads and blacklisted regions using Picard (v2.6.0) (http://broadinstitute.github.io/picard) and Bedtools (v2.13.3),[117] respectively; and iv) conversion of bam files into bigwig files for data visualization using Deeptools. Peaks were called using MACS2 (v.2.1.0)[120] with the following settings: –bw=300 –keep-dup all –qvalue 0.01. Mouse naked and tagmented DNA was used as control input as previously described.[139] Given that ChIP-seq replicates were highly correlated, the union of peaks found in both replicates were used for further analyses. HNF1A-bound regions were annotated as transcriptional start site (TSS) proximal, TSS-distal, intronic, exonic, or intergenic using Homer (v4.10).[121] HNF1A-bound genes or direct targets were determined by assigning peaks to their closest gene using bedtools (v2.13.3)[117] closest.

HNF1A binding site specificity was ascertained by performing ChIP-seq with two monoclonal antibodies (Cell Signalling, Santa Cruz, see key resources table), raised against an amino terminal synthetic peptide, or a recombinant protein with residues 80-284, resulting in highly correlated binding signals highly enriched in HNF1 recognition sequences (Figures S2B–S2E).

Motif analysis

Known and *de novo* motif enrichment analysis for HNF1A-bound regions within promoters and enhancer was performed using HOMER with default settings (200 bp around HNF1A peak center) and using H3K27ac peaks as background sequences. HNF1 position weight matrixes were obtained from HOCOMOCO,[122] and used to assess the presence of HNF1A binding sequence motifs in ChIP-seq peaks.Motif enrichment analysis for A1CF was carried out employing rMAPS[116] (using as input rMATS output files) -with default settings.

Data visualization

Bed and bigwig files from RNA-seq and ChIP-seq experiments were visualized in the Genome Browser (http://genome.ucsc.edu/). ggplot2 R package[123] was used to generate complex plots whereas simpler plots were created with GraphPad Prism 7. GSEA plots were obtained from Genepattern[124] and RBP maps from rMAPS.[116] Cartoons and models have been created with BioRender.com. Tissue expression data were obtained from the GTEx Portal.[74]

VASA-seq single-cell transcriptome and differential splicing analysis

Human Cell Atlas ESPACE consortium VASA-seq[66] single-cell transcriptome data was obtained from primary human pancreatic islets from 11 donors (5 T2D, 6 non-T2D), and described in detail elsewhere (manuscript in preparation). To enable comparisons, VASA-seq reads were re-aligned in parallel with *A1CF*^{KO} and *HNF1A*^{KO} RNA-seq reads to the human (GRCh38 gencode v.34) genomes using STAR (v2.7.11),[107] excluding the *INS* gene from the alignment. Aligned VASA-seq data was processed using Seurat 5.0.1[125] by sample. After considering a range of 1,000 to 10,000 genes, we selected 2,000 genes highly variable genes. We clustered the data using Seurat[125] Louvain algorithm with a resolution of 0.5, then merged all samples, and performed integration with Harmony.[126] Major endocrine cell types were annotated with marker genes, namely *MAFA*, *GCG*, *SST* and *PPY* for β, α, δ and γ cells, respectively. Differential alternative splicing was examined with rMATS (turbo 4.3.0)[50] using default settings except for the –variable-read-length option. To compare EndoC-βH3 *A1CF*^{KO} and VASA-seq splicing patterns, we processed both datasets with rmats software using the same parameters, and then joined alternative splicing events by their exact rmats coordinates, using dplyr::inner_join() function, and filtered for minimum amounts of read in each experiment (10 reads in at least 2/3 of replicates in EndoC-βH3 and 10 reads for each cell group tested in VASA-seq). We separately compiled a list of alternative splicing events that are shared in VASA-seq subtypes, *A1CF*^{KO}, and *HNF1A*^{KO} cells, for which we identified differentially spliced events of the same type (MXE, SE, A5SS, A3SS) containing overlapping outermost coordinates in the three datasets.

Co-expression analysis

VASA-seq[66] single cell transcriptome data from the same 11 donors were processed separately for co-expression analysis. A total of 18,242 genes expressed in >5% of cells with TPM >1, were selected. 1,575 cells (i) labeled as β-cells as a result of the expression of key marker genes in the Louvain-derived single-cell clusters and (ii) expressing at least 2% of the selected genes were used for the co-expression analysis. Transcript counts for these cells and genes were normalized using Normalisr,[127] which infers normalized log mRNA expression levels that partly address the count sparsity of conventional log-TPM counts. All gene (Pearson's) correlation coefficients reported were computed using the normalized counts. Matched control gene sets were generated to be three times the size of the respective gene set of interest. For each gene of interest, three genes at random were sampled from the filtered gene list such that they were within 6 positions from the gene in terms of TPM ranking.

QUANTIFICATION AND STATISTICAL ANALYSIS

Replicate numbers are described in figure legends. RNA-seq or RT-qPCR experiments in islets or cell lines were carried out in a single experiment with indicated biological replicates. The significance of RT-qPCR experiments was determined using a two-tailed t-test. Fisher's exact test (GeneOverlap R package) was performed to examine gene set overlaps, using all expressed genes (Log2 TPM > 2.5) for each tissue as background, as well as for differential arginine responsiveness of β-cell electrical activity. Bar graphs depict means ± s.e.m. If not stated otherwise, statistical analysis for comparison of two groups was performed by unpaired t-test (two-tailed) and for more than two groups by two-way analysis of variance (ANOVA) followed by Bonferroni's correction using GraphPad Prism 7.0 software. For immunofluorescence staining representative images of at least two independent experiments with similar results have been provided. Sample sizes were determined on the basis of previous experiments using similar methodologies.

Visualization of genetic associations

Regional association plots at the *A1CF* locus for RG and T2D were created using LocusZoom v1.4[140] in R-3.6.1. We used summary statistics data of European-ancestry specific meta-analyses for RG[68] and T2D.[67]

Genetic fine-mapping

We employed a Bayesian approach[141] to construct a credible set with 99% posterior probability of harboring the causal variant at the *A1CF* T2D association. We first defined a 500 kb genomic region centered on the *A1CF* T2D association, encompassing all genetic variants with MAF $\geq$ 1% and LD $r^2 \geq 0.1$ with the lead rs12570156 variant. LD correlation measures were computed using individuals of European descend from 1000 Genomes Project (http://www.1000genomes.org/). Subsequently, we calculated approximate Bayes' Factors (ABF)[142] for each variant based on the effect size and the standard error, derived from a recent large-scale T2D meta-analysis (using data from individuals of European descend). We then computed posterior probabilities and ranked genetic variants in descending order of ABF to estimate cumulative posterior probabilities. Genetic signals were added to the credible set until exceeding the 99% cumulative posterior probability. We obtained 99% credible sets for the *A1CF* rs61856594 association for random glucose as reported in Lagou et al.[68]

Colocalization analysis

We conducted colocalization analysis at the *A1CF* locus between (i) random glucose and T2D associations, as well as (ii) random glucose genetic associations and islet *cis* eQTLs.[71] We employed COLOC (v.5.2.3)[131] to examine potential colocalization between each pair of traits within +/- 500 kb around the lead random glucose association, using the fraction of common variants between the two traits under comparison. We next evaluated with COLOC the posterior probability of the following five hypothesis at the *A1CF* locus for each comparison: H_0, no association; H_1, RG association only; H_2, $\text{trait}_{i/ii}$ association only; H_3, both random glucose and $\text{trait}_{i/ii}$ association, but not colocalized and H_4, both random glucose and $\text{trait}_{i/ii}$ association and colocalized. Finally, colocalization events were visualized using LocusCompareR 1.0.0 in R-3.6.1. SNP linkage for coloring genetic variants was determined using the LDpair and LDproxy functions from the R package LDlinkR and a European based population as the LD reference panel.[130]

Transcriptome-Wide Association Studies

We utilized the FUSION[70] software to conduct transcriptome-wide association studies of random glucose. Leveraging pre-computed SNP-weights for islet gene expression (trained on a panel of 399 human islet samples with genotype and transcriptome data available[71]), we employed the *FUSION_assoc_test.R* script to assess the association between imputed islet gene expression and random glucose. This method enables using summary statistics data, rather than individual-level genetic data, to predict islet gene expression in the RG GWAS cohort. We aligned the European-based random glucose meta-analysis to the genomic coverage of the panel of 399 human islet samples (~6.5 common genetic variants). We applied multiple-test correction to the resulting TWAS *P*-values using Bonferroni, considering a total of 2,851 features. FUSION was also run in conjunction with the COLOC software to compute approximate colocalization statistics based on the marginal FUSION weights. This enabled the identification and exclusion of TWAS signals that lacked sufficient evidence for colocalization evidence and are hereby confounded by linkage (COLOC PP4 < 0.6).